A&A 508, 1285–1299 (2009)
DOI: 10.1051/0004-6361/200912583

Astronomy & Astrophysics

An updated survey of globular clusters in M 31

III. A spectroscopic metallicity scale for the Revised Bologna Catalog[⋆,⋆⋆]

S. Galleti, M. Bellazzini, A. Buzzoni, L. Federici, and F. Fusi Pecci

INAF – Osservatorio Astronomico di Bologna, via Ranzani 1, 40127 Bologna, Italy
e-mail: [silvia.galleti;michele.bellazzini;luciana.federici;alberto.buzzoni;flavio.fusipecci]@oabo.inaf.it

Received 27 May 2009 / Accepted 17 September 2009

ABSTRACT

Aims. We present a new homogeneous set of metallicity estimates based on Lick indices for the old globular clusters of the M 31 galaxy. The final aim is to add homogeneous spectroscopic metallicities to as many entries as possible of the Revised Bologna Catalog of M 31 clusters[⋆⋆⋆], by reporting Lick index measurements from any source (literature, new observations, etc.) on the same scale.
Methods. New empirical relations of [Fe/H] as a function of [MgFe] and Mg2 indices are based on the well-studied galactic globular clusters, complemented with theoretical model predictions for $-0.2 \leq$ [Fe/H] $\leq +0.5$. Lick indices for M 31 clusters from various literature sources (225 clusters) and from new observations by our team (71 clusters) have been transformed into the Trager et al. system, yielding new metallicity estimates for 245 globular clusters of M 31.
Results. Our values are in good agreement with recent estimates based on detailed spectral fitting and with those obtained from color magnitude diagrams of clusters imaged with the Hubble Space Telescope. The typical uncertainty on individual estimates is $\simeq \pm 0.25$ dex, as resulted from the comparison with metallicities derived from color magnitude diagrams of individual clusters.
Conclusions. The metallicity distribution of M 31 globular cluster is briefly discussed and compared with that of the Milky Way. Simple parametric statistical tests suggest that the distribution is probably not unimodal. The strong correlation between metallicity and kinematics found in previous studies is confirmed. The most metal-rich GCs tend to be packed into the center of the system and to cluster tightly around the galactic rotation curve defined by the HI disk, while the velocity dispersion about the curve increases with decreasing metallicity. However, also the clusters with [Fe/H] < -1.0 display a clear rotation pattern, at odds with their Milky Way counterparts.

Key words. galaxies: individual: M 31 – galaxies: star clusters – catalogs – Local Group

1. Introduction

The concept of simple stellar population (SSP) has proven to be a very fruitful tool for the study of virtually any kind of stellar system (Renzini & Buzzoni 1986; Renzini & Fusi Pecci 1988, hereafter RFP88). An SSP is completely characterized by only four "parameters", (a) mass; (b) chemical composition; (c) age; and (d) mass function, which determine the mass to light ratio (M/L) of the SSP once fixed the age and the chemical composition (see RFP88, for further possibly relevant variables that are not considered at zero-approximation). As a further simplification, the chemical composition is typically represented by two main parameters, i.e. the helium abundance (Y) and the total abundance of elements heavier than helium, usually parametrized by the iron abundance [Fe/H] (see, for instance (Zinn & West 1984, ZW84; Tantalo & Chiosi 2004b,a, and references therein). Even if the abundance of the so-called α-elements has been the subject of increasing interest in the past two decades (McWilliam 1997; Thomas et al. 2004; Tantalo & Chiosi 2004a; Gratton et al. 2004) [Fe/H] remains the main parameter for ranking stars and/or stellar populations according to their abundance of heavy elements.

In the study of globular clusters (GCs), which are the best approximation of an SSP in nature, the metallicity is a key parameter that is also needed to infer ages and age differences (see, for example RFP88 and Carretta & Gratton 1997, and references therein). The knowledge of the metallicity of a large sample of GCs in a given galaxy allows one to search for metallicity gradients and for distinct subpopulations of GCs (as in the Milky Way (MW) Zinn 1985; and in many external galaxies Brodie & Strader 2006) and, in general, to obtain crucial information on the early phases of the formation and chemical enrichment of the parent galaxy.

While modern instrumentation has allowed determination of the detailed abundance of several elements in single stars belonging to GCs of the MW (see Sneden 2005; Gratton et al. 2004; Carretta et al. 2008), the metallicities of extragalactic GCs must be obtained from their integrated colors and/or spectra, by comparison with Galactic templates and/or theoretical models (Brodie & Strader 2006). Several broad-band integrated colors are fairly sensitive to metallicity and relatively easy to measure for clusters out to very large distances. However, they suffer from the well-known age-metallicity degeneracy (RFP88), *and* they may be badly affected by the reddening due to extinction by interstellar dust. While the foreground extinction associated

⋆ Based on observations made at La Palma, at the Spanish Observatorio del Roque de los Muchachos of the IAC, with the William Herschel Telescope of the Isaac Newton Group and with the Italian Telescopio Nazionale Galileo (TNG) operated by the Fundación Galileo Galilei of INAF. Also based on observations made with the G.B. Cassini Telescope at Loiano (Italy), operated by the Osservatorio Astronomico di Bologna (INAF).

⋆⋆ Appendices are only available in electronic form at http://www.aanda.org

⋆⋆⋆ RBC Version 4 available at: www.bo.astro.it/M31

with the dust layers residing in our own Galaxy may be somehow constrained by observations and modeled (Schlegel et al. 1998), the extinction intrinsic to external galaxies is largely unknown. On the other hand, spectral indices based on the strength of an absorption feature with respect to the surrounding continuum also suffer from the age-metallicity degeneracy (to different degrees, see Worthey 1994) but they are essentially unaffected by extinction (MacArthur 2005), a very desirable characteristic. The most widely used spectral indices were originally defined by Burstein et al. (1984) and Faber et al. (1985) at the Lick Observatory. These authors defined a set of indices that measure the strength of the most pronounced absorption features that are seen in the integrated low-resolution spectra of stellar systems at optical wavelengths. The use of Lick indices became widespread because they are easy to measure; as a consequence, they were also included as standard predictions in all theoretical models of SSP (see, for example, Buzzoni et al. 1992, 1994; Worthey 1994; Bruzual & Charlot 2003, hereafter BC03; Tantalo & Chiosi 2004b; Thomas et al. 2003, hereafter TMB).

The M 31 galaxy is an ideal target for studying GCs. It is nearby and it has a large cluster population (∼3 times more than the MW). The GC system of M 31 has been intensively studied in the past and several authors have used Lick indices to constrain the age and the metallicity of clusters in the Andromeda galaxy.

Integrated-light spectroscopy of M 31 GCs was pioneered by van den Bergh (1969) who found that the GC system of this galaxy extends to higher metallicities than in the MW. In an important contribution, Burstein et al. (1984) comprehensively discussed other interesting differences between GCs in M 31 and in the MW. In particular they showed that M 31 clusters have significantly stronger Hβ and CN absorption indices at a given metallicity. In a series of papers, Brodie & Huchra (1990, 1991) and Huchra et al. (1991) studied the metallicity distribution of M 31 GCs using an extensive sample of integrated spectra and line indices. They found that the properties of the M 31 GC system are broadly similar to the MW one, but they confirmed the presence of a high-metallicity tail with no counterpart in our Galaxy. They found that the mean metallicity [Fe/H] was −1.2, and identified a weak metallicity gradient as a function of projected radius. From the distribution of integrated colors, Barmby et al. (2000) found evidence that the M 31 GC system may have a bimodal metallicity distribution (like the MW, Zinn 1985), with peaks at [Fe/H] ∼ −1.4 and [Fe/H] ∼ −0.6. Moreover, they found that the $(V-K)_0$ color distribution was best modeled by assuming three modes in the metallicity distribution, instead of one or two. Finally, they found a small radial metallicity gradient and no correlation between cluster luminosity and metallicity in M 31 GCs. Perrett et al. (2002) have produced a total sample of about 200 spectroscopic metallicities of M 31 GCs, calibrating Lick indices measured in their own system versus the metallicity of M 31 clusters in common with Huchra et al. (1991) (so they used a set of *secondary* calibrators). They confirm the bimodality in the metallicity distribution and reported that the metal-rich clusters have a higher rotation amplitude with respect to metal-poor ones, while both groups are known to rotate faster than their Galactic counterparts. Moreover, they found evidence of a radial metallicity gradient in the metal-poor population of M 31 out to ∼60′ from the galaxy center.

Metallicity (and age) estimates for various samples of M 31 clusters obtained by fitting spectra with theoretical SSP models have recently been presented by Beasley et al. (2005) and Puzia et al. (2005). Beasley et al. (2005) studied a sample of 23 M 31 GCs with very high signal-to-noise (S/N) spectra, seventeen of which were found to be old and to span a wide range of metallicity, while the remaining six were classified as intermediate-age clusters. Puzia et al. (2005) present the metallicity of 70 GCs (including those studied by Beasley et al. 2005) finding a bimodal distribution with peaks at [Z/H] ∼ −1.66 (±0.05) and [Z/H] ∼ −0.45 (±0.04) dex with dispersions 0.23 and 0.29 dex, respectively[1].

More recently, Lee et al. (2008) have merged the metallicities from Barmby et al. (2000) and Perrett et al. (2002) with their own estimates from the line indices measured from WIYN/Hydra spectra. They find that a bimodal and trimodal distribution are statistically preferable to a unimodal metallicity distribution at a confidence level of 99.8%. Fan et al. (2008) assembled metallicities from the literature and with estimates derived from integrated colors to obtain a global metallicity distribution of M 31 GCs. They find a bimodal distributions with peaks at [Fe/H] ∼ −1.7 and ∼−0.7 dex with mean [Fe/H] = −1.21 dex, but show that three-group fits are also statistically acceptable. They find a metallicity gradient as a function of projected radius for the metal-poor GCs, but no gradient for the metal-rich GCs.

The brief summary of modern studies above underlines the high degree of heterogeneity of the available material. The various sets of estimates are obtained from observables that are different in nature (integrated spectral indices or colors) and are based on different calibrations (empirical, semi-empirical, or theoretical; using primary or secondary calibrators). Even the actual definition of the same Lick indices varies from author to author; thus, in general, the presented calibrations are only valid for a given observational set-up and definition. In these circumstances it is clear that joining different sets of metallicity estimates may be quite dangerous as it may lead to a poor degree of self-consistency in the final merged set.

We have assembled and we continuously maintain and update a database of parameters of confirmed and candidate clusters[2] in M 31, the Revised Bologna Catalog of M 31 GCs (RBC, Galleti et al. 2004, 2006a, 2007). Because we want to add a reliable metallicity estimate to the confirmed clusters in the RBC, we need to devise the operational protocol for transforming the actual measures provided in the literature (as, for example, already available and future sets of Lick indices for M 31 clusters) into a unique homogeneous metallicity scale. In this paper, we describe the construction of this new homogeneous metallicity scale for M 31 GCs based on Lick line indices. Having set and tested the new scale, we present new metallicity estimates for 245 M 31 GCs.

The plan of the paper is as follows. In Sect. 2, we describe the rationale and the procedure for constructing the new metallicity scale. In Sect. 3, we report on the sample of M 31 GC spectra that we have obtained and reduced, and from which we estimated Lick indices. We also describe how we collected Lick indices for M 31 GCs from the literature and how we have tied all of them to the same homogeneous system. Finally, we derive the new values of the metallicities and, in Sect. 4, compare our scale with previous metallicity estimates. In Sect. 5, we present and discuss the metallicity distribution of the M 31 GC system and the correlations between metallicity and kinematics.

[1] [Z/H] is defined as [Fe/H] + 0.94[α/Fe] taken from Thomas et al. (2003; see also Trager et al. 2000).

[2] We also keep lists of targets previously suggested as candidate M 31 GCs and later found to be objects of different natures, like distant galaxies, foreground stars, regions HII etc., see Galleti et al. (2004, 2006a, 2007).

2. An empirical metallicity scale

The construction of a metallicity scale must be driven by a list of basic requirements and a number of methodological/technical choices to achieve them, as well as some trade-offs between different possibilities. In particular, we identified the following ranked list of desiderata.

1. The scale must be consistent with at least one of the main metallicity scales currently used for the Galactic GCs, like Zinn & West (1984, ZW84) or Carretta & Gratton (1997).
2. The scale must be calibrated on empirical templates. The agreement with theoretical predictions is clearly desirable but is not a *must*, because theoretical models have problems and uncertainties of their own (Tantalo & Chiosi 2004a,b), while the chemical abundances of many Galactic GCs are known in great detail (Carretta et al. 2008).
3. The observables that are used to settle the scale must be as sensitive to the abundance of heavy elements as possible,operationally well-defined, and easy to measure out to large distances with currently available instrumentation.

Several authors have studied and discussed in detail the sensitivity of the various Lick indices to the abundance of various elements and to other parameters (see González 1993; Worthey 1994; Worthey et al. 1994; Worthey & Ottaviani 1997; Buzzoni et al. 1992; Buzzoni 1995b; Trager et al. 1998; Thomas et al. 2004, 2003; Tantalo & Chiosi 2004a,b, and references therein). Even if several indices are fairly sensitive to metallicity, they are not necessarily suitable as the basis of a general purpose metallicity scale. As an extreme example, the Hβ index is very sensitive to metallicity but also very sensitive to age, making it a misleading metallicity indicator, in general. Fe4648, Fe5015, Fe5709, and Fe5782 have been indicated as very good metallicity indicators, but none of these absorption features seems ideal for reliable metallicity determinations. Fe4648 was found to be sensitive to C, O, Mg, and Si, so it does not seem to trace any iron peak element. Fe5015 is mostly sensitive to iron, but it can be affected by [OIII] emission. Fe5709 and Fe5782 are weak features which require very high S/N spectra to be reliably measured. There is general consensus that the most reliable (and easy to measure) iron-sensitive Lick indices are Fe5270 and Fe5335, as both measure predominantly strong iron lines. However all these features are relatively weak in most old SSP spectra with respect to the Mg features that are parametrized by the Mg2 and Mgb indices, both of which are shown to correlate very well with [Fe/H] (Worthey 1994, 1996).

As it become clear that old stellar populations (like GCs and classical elliptical galaxies) are characterized by an enhancement of α elements (N, O, Mg, Ca, Na, Ne, S, Si, Ti), or, better, by an iron deficiency with respect to the abundance pattern of the Sun, the impact of [α/Fe] on Lick indices has been the subject of detailed study (see Trager et al. 2000; Tantalo & Chiosi 2004a; Thomas et al. 2004, and references therein). To reduce the influence of [α/Fe] variations on age and metallicity determinations, González (1993) introduced the [MgFe] index, $[\mathrm{MgFe}] = \sqrt{\mathrm{Mgb} \cdot \langle \mathrm{Fe} \rangle}$ with $\langle \mathrm{Fe} \rangle = (\mathrm{Fe5270} + \mathrm{Fe5335})/2$, which appears to be very sensitive to the total metallicity while minimizing the dependency on [α/Fe] (see Thomas et al. 2004, 2003, for discussion).

After many tests using several indices, we decided to base our scale on four indices: three of them (Mgb, Fe5270, and Fe5335) are combined into [MgFe], the other is Mg2 (see Appendix B, in online edition). Mg2 has become a standard "metallicity" indicator for the integrated spectra (see i.e. Buzzoni et al. 1992). We found that [MgFe] and Mg2 provide the most consistent and strong correlations with [Fe/H] in the ZW84 scale, once the Trager et al. (1998, hereafter T98) definitions of the Lick indices are adopted. Therefore, to obtain a metallicity estimate on a reliable and homogeneous scale, the indices must be measured according to the T98 definitions and transformed into the T98 reference frame using a set of stars/stellar systems in common with T98 as standard calibrators (see Sect. 3, below). Operationally, when the spectrum of a given cluster has enough signal-to-noise and wavelength coverage to allow a reliable measure of all the involved indices, including Fe5270 and Fe5335, the estimates of [Fe/H] can be obtained from [MgFe]. A valid metallicity estimate can be obtained even if reliable measures of Fe5270 and Fe5335 are lacking; the use of both the assumed indicators is clearly preferable, but Mg2 alone is sufficient.

2.1. The calibrators

To fulfil simultaneously the requirements #1 and #2 above, we decided to adopt Galactic GCs with metallicities in the ZW84 scale as fundamental calibrators. All the metallicity values for MW GCs adopted here were taken from ZW84 and Armandroff & Zinn (1988). It is clear that the choice of the calibrators implies that the scale is only valid for old populations having a similar degree of enhancement in the abundance of α-elements with respect to the Sun (see Pritzl et al. 2005). We use theoretical SSP models to explore the effective range of ages and chemical compositions in which our calibration can be considered valid.

We searched in the literature to assemble the largest possible sample of Galactic GCs with well known metallicity and well-measured Lick indices from high S/N spectra in the T98 system or that can be easily transformed into this system. First of all we took the data for 17 Galactic GCs provided by T98 themselves, by definition in the T98 system. The original spectra were obtained by Burstein et al. (1984) with the image dissector scanner (IDS) at the 3 m Shane Telescope of the Lick Observatory, and the absorption-line indices were measured again by T98. Next, we incorporated the new data for 41 GCs from spectra obtained with the Blanco 4 m telescope by Schiavon et al. (2005, hereafter S05)[3]. We measured the needed indices (Mg2, Mgb, Fe5270, and Fe5335) from the Schiavon et al. spectra as described in detail in Sect. 3.1, below. We used the 8 clusters in common with the T98 to derive a simple least square fit converting indices from the S05 to the T98 system (using OLS($X|Y$), according to Isobe et al. (1990); see Fig. 1). The derived values of the (a, b) coefficients for the various indices are reported in Table 1.

Indices for further 3 GCs were taken from Beasley et al. (2004, hereafter B04) who re-measured Lick indices for 12 GCs spectra obtained by Cohen et al. (1998). The coefficients given in Table 2, derived by least-square fitting for clusters in common, as above, were used to convert the B04 indices into the T98 system. Figure 2 compares the values of the indices from the sample obtained by joining the data from T98 and S05 with the B04 sample, after transformation to the T98 system. The plots show that the set of measures we have assembled is *very* homogeneous: any residual systematic and/or random scatter is ∼5% of the range spanned by the index, or smaller.

We merged all the sources described above into a global sample comprising 53 Galactic GCs with metallicities $-2.24 \leq [\mathrm{Fe/H}] \leq -0.23$ on the ZW84 scale. In case of multiple

[3] See http://www.noao.edu/ggclib

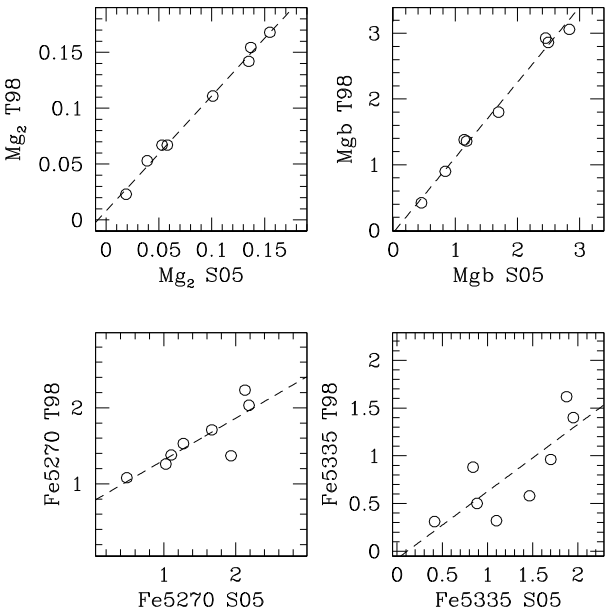

Fig. 1. Comparison of passband measurements from S05 spectra and original Lick data for 8 Galactic GCs. Dashed lines show the least-square fit relations.

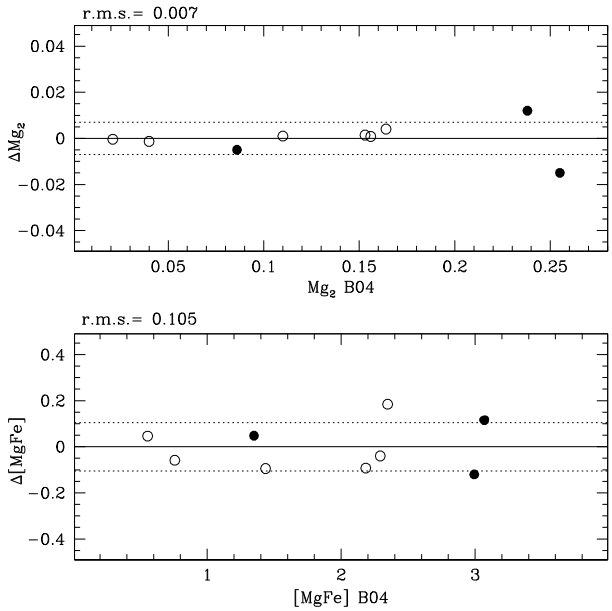

Fig. 2. Comparison of the metallicity line indices adopted with the B04 values transformed to the T98 system (T98 data: open circles; S05 data: filled circles). The rms of the distributions are also reported.

Table 1. Linear fit coefficients to convert the Schiavon (S05) indices into the Lick system.

Index	*a*	*b*	rms
Mg2	0.008	1.029	0.004
Mgb	–0.034	1.145	0.098
Fe5270	0.761	0.551	0.199
Fe5335	–0.079	0.704	0.275

Table 2. Linear fit coefficients to convert the Beasley (B04) indices into the Lick system.

Index	*a*	*b*	rms
Mg2	–0.008	1.002	0.006
Mgb	–0.051	1.076	0.187
Fe5270	0.377	0.757	0.217
Fe5335	–0.009	0.872	0.205

measures we adopted one single source according to the following ranking: T98, S05, and B04. Lick indices, source and uncertainties for all sample adopted are given in Table 3.

As recalled in Sect. 1, it has long been known that M 31, as do other giant galaxies (see Harris et al. 1992), hosts GCs that are significantly more metal rich than found in the MW, possibly up to super-solar metallicities. To extend the range of applicability of our metallicity scale at the super solar regime – where we lack observed calibrators – we complemented our sample with a suitable set of several models for old SSPs (i.e. 12−12.5 Gyr, see Gratton et al. 1997), with metallicity in the range $-0.3 \leq$ [Fe/H] $\leq +0.5$. In particular, the theoretical predictions by Buzzoni (1989), Worthey (1994), Bruzual & Charlot (2003), Thomas et al. (2004), and Tantalo & Chiosi (2004b) have been considered. The simultaneous use of models from different authors provided a confident estimate of the internal uncertainty of the theoretical framework, intrinsic to the different input physics among the various theoretical synthesis codes. Therefore, to fit our calibrating relations, we adopted a composite sample made by the empirical set of 53 Galactic GC in the range $-2.5 \leq$ [Fe/H] < -0.2, plus the theoretically predicted index values described above, considered as observed points, in the range $-0.2 \leq$ [Fe/H] $\leq +0.50$. While the agreement between the observed points and the models predictions is quite good over the whole metallicity range covered by Galactic GCs (see Fig. 5, below), the reader must be aware that the metallicity scale proposed here is not constrained by empirical calibrators in the solar and super-solar regimes.

To avoid confusion resulting by plotting many different symbols in such a restricted range of metallicities, in Fig. 3 we simply plot a sketch of the envelope enclosing all the theoretical points that were considered in the calibration.

The two best-fit relations are shown in Fig. 3; they are the following second-order polynomials represented by

$$[\mathrm{Fe/H}]_{[\mathrm{MgFe}]} = -2.563 + 1.119[\mathrm{MgFe}] - 0.106[\mathrm{MgFe}]^2 \pm 0.15 \text{ dex, rms} \quad (1)$$

$$[\mathrm{Fe/H}]_{\mathrm{Mg_2}} = -2.276 + 13.053\mathrm{Mg_2} - 16.462\mathrm{Mg_2^2} \pm 0.15 \text{ dex, rms.} \quad (2)$$

Equations (1) and (2) are the fundamental calibrating relations of the proposed metallicity scale. When all the needed observables are available, the final metallicity value is obtained from Eq. (1); otherwise one recurs to Eq. (2).

The internal consistency of the adopted scale is verified in Fig. 4, where the original metallicity values of the calibrating clusters are compared with those obtained with our calibrations. The r.m.s. scatter is ≃0.15 dex. Figures 3 and 4 suggest that our scale is less sensitive to metallicity variations and more uncertain at the metal-poor end, for [Fe/H] $\lesssim -1.9$. This is a general characteristic of scales based on integrated Lick indices (see, for example Faber et al. 1985; Cohen et al. 2003) and must be taken into account when very metal poor clusters are considered.

The effects of age assumptions are explored in Fig. 5, where we compare our $\mathrm{Mg_2}$ data with an illustrative set of theoretical models from several population synthesis codes. In particular, we relied on the models by Buzzoni (1989, 1995a),

Table 3. Lick indices for MW GCs, computed with the passband definitions of Trager et al. (1998) and shifted in this system.

Cluster	Mg_2 mag	eMg_2 mag	Mg*b* Å	eMg*b* Å	Fe5270 Å	eFe5270 Å	Fe5335 Å	eFe5335 Å	Source[a]
NGC 104	0.153	0.007	3.022	0.013	1.925	0.015	1.256	0.017	2
NGC 1851	0.075	0.009	1.396	0.024	1.606	0.026	0.820	0.030	2
NGC 1904	0.039	0.009	0.788	0.035	1.297	0.039	0.516	0.046	2
NGC 2298	0.033	0.012	0.907	0.063	1.154	0.071	0.391	0.081	2
NGC 2808	0.075	0.007	1.374	0.015	1.613	0.017	0.838	0.019	2
NGC 3201	0.063	0.009	1.836	0.032	1.407	0.036	0.583	0.041	2
NGC 5024	0.039	0.010	0.830	0.295	0.370	0.268	0.550	0.281	1
NGC 5272	0.040	0.008	1.010	0.235	1.060	0.220	0.410	0.213	1
NGC 5286	0.048	0.009	0.903	0.023	1.287	0.026	0.526	0.030	2
NGC 5904	0.067	0.010	1.380	0.300	1.530	0.282	0.320	0.257	1
NGC 5927	0.197	0.009	3.885	0.035	2.183	0.039	1.549	0.044	2
NGC 5946	0.056	0.009	0.844	0.058	1.337	0.063	0.410	0.072	2
NGC 5986	0.048	0.009	0.900	0.026	1.278	0.029	0.465	0.034	2
NGC 6121	0.081	0.009	1.677	0.023	1.467	0.026	0.705	0.030	2
NGC 6171	0.111	0.015	1.800	0.447	1.710	0.420	0.580	0.427	1
NGC 6205	0.039	0.006	0.725	0.140	0.976	0.131	0.609	0.136	1
NGC 6218	0.067	0.011	1.360	0.338	1.380	0.317	0.500	0.316	1
NGC 6235	0.079	0.012	1.188	0.068	1.599	0.074	0.855	0.084	2
NGC 6254	0.050	0.009	0.861	0.023	1.315	0.026	0.495	0.029	2
NGC 6266	0.082	0.007	1.638	0.015	1.555	0.017	0.821	0.019	2
NGC 6284	0.084	0.009	1.562	0.037	1.475	0.041	0.730	0.047	2
NGC 6229	0.077	0.013	1.100	0.398	0.980	0.372	0.390	0.356	1
NGC 6304	0.180	0.009	3.545	0.035	2.056	0.039	1.399	0.044	2
NGC 6316	0.151	0.009	2.896	0.045	1.864	0.049	1.033	0.055	2
NGC 6333	0.040	0.009	0.748	0.028	1.213	0.032	0.336	0.036	2
NGC 6342	0.115	0.012	2.737	0.081	1.663	0.091	1.099	0.102	2
NGC 6352	0.157	0.009	3.198	0.044	1.867	0.049	1.329	0.056	2
NGC 6341	0.021	0.005	0.800	0.176	0.448	0.161	0.323	0.151	1
NGC 6356	0.168	0.009	3.060	0.251	2.034	0.236	1.400	0.263	1
NGC 6362	0.103	0.009	2.099	0.034	1.567	0.038	0.741	0.044	2
NGC 6388	0.138	0.007	2.393	0.017	2.029	0.018	1.335	0.021	2
NGC 6440	0.217	0.010	3.443	0.080	2.131	0.130	1.412	0.130	3
NGC 6441	0.159	0.009	2.921	0.020	2.043	0.022	1.383	0.025	2
NGC 6522	0.096	0.009	1.543	0.032	1.597	0.035	0.803	0.039	2
NGC 6528	0.250	0.009	4.377	0.042	2.421	0.046	1.884	0.051	2
NGC 6539	0.185	0.010	2.970	0.100	1.995	0.150	1.246	0.150	3
NGC 6544	0.086	0.009	0.950	0.046	1.564	0.049	0.764	0.055	2
NGC 6553	0.240	0.009	4.300	0.042	2.418	0.045	1.751	0.051	2
NGC 6569	0.127	0.009	2.329	0.049	1.654	0.054	0.967	0.061	2
NGC 6624	0.154	0.008	2.860	0.240	2.233	0.226	1.618	0.253	1
NGC 6626	0.083	0.009	1.554	0.025	1.445	0.027	0.743	0.031	2
NGC 6637	0.142	0.010	2.926	0.288	1.369	0.269	0.961	0.292	1
NGC 6638	0.124	0.009	2.184	0.035	1.736	0.038	1.021	0.043	2
NGC 6652	0.107	0.009	2.381	0.030	1.722	0.034	0.957	0.039	2
NGC 6712	0.112	0.015	1.570	0.431	1.410	0.405	0.690	0.423	1
NGC 6723	0.075	0.009	1.554	0.031	1.462	0.035	0.636	0.040	2
NGC 6752	0.044	0.009	0.924	0.025	1.264	0.029	0.445	0.033	2
NGC 6760	0.217	0.010	3.496	0.080	2.116	0.140	1.455	0.130	3
NGC 6838	0.157	0.010	2.628	0.295	1.774	0.277	1.855	0.314	1
NGC 6981	0.064	0.014	0.810	0.421	1.280	0.397	0.450	0.389	1
NGC 7006	0.052	0.012	0.665	0.352	0.529	0.326	0.633	0.344	1
NGC 7078	0.023	0.007	0.420	0.211	1.080	0.201	0.310	0.182	1
NGC 7089	0.053	0.008	0.900	0.242	1.260	0.228	0.880	0.245	1

[a] Dataset label: 1 – Trager et al. (1998); 2 – Schiavon et al. (2005); 3 – Beasley et al. (2004).

Worthey et al. (1994), Girardi et al. (2000), Bruzual & Charlot (2003), and Tantalo & Chiosi (2004b). The upper panel of the figure displays a collection of the 12 Gyr model predictions, while the expected shift in the theoretical loci when moving to younger ages is estimated in the lower panel. One can see that any change in age, say from 12 to 5 Gyr, is reflected in a shallower slope of the theoretical [Fe/H] vs. Mg_2 calibration, as a consequence of a larger offset ($\Delta\ Mg_2 \sim -0.05$ mag) at solar metallicity. On the other hand, any enhancement in the [α/Fe] element partition results in a (roughly) solid shift of the curve shelf to correspondingly lower values of [Fe/H], as sketched on the plot.

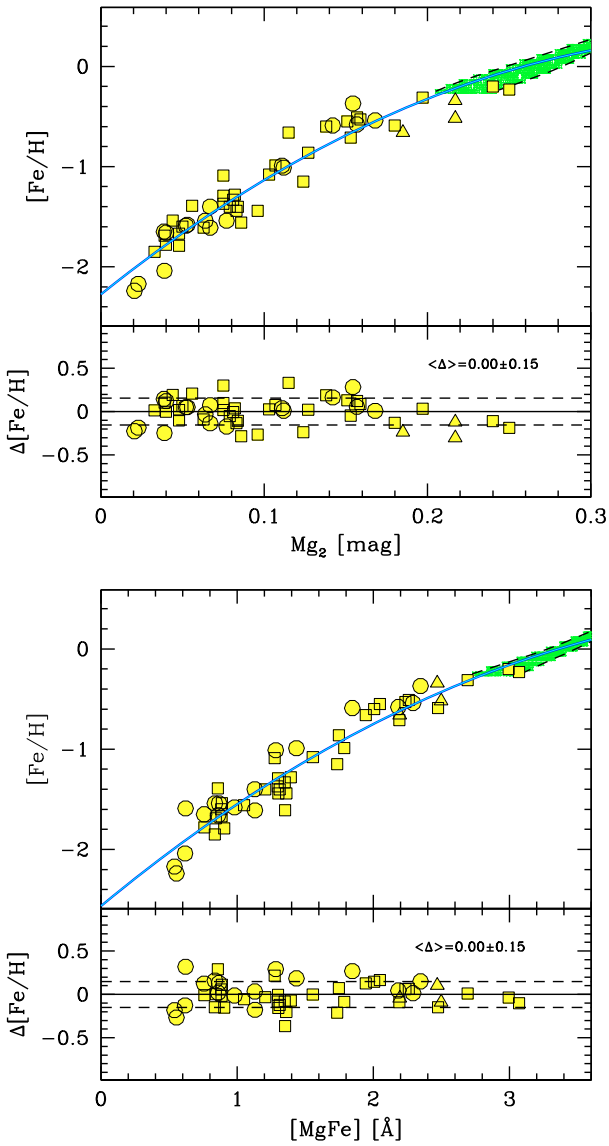

Fig. 3. The adopted calibrations for Mg2 and [MgFe] vs. [Fe/H] (continuum lines) superposed on the accounted set of Galactic GCs from T98 (dots), S05 (squares), and B04 (triangles). The shaded regions at super-solar metallicity are the envelope of the theoretical predictions from several SSP models, as discussed in the text. A comparison between the empirical metallicities and ZW84 with the mean differences and rms are also reported in *the lower panels*. The dashed lines enclose the rms. The color figures are available in the electronic edition.

The comparison between our empirical calibrating relations and the model predictions reveal that the application of our method to clusters as young as 5 Gyr, in the metallicity range $-2.0 < [Fe/H] < 0.0$, would lead to systematic errors in the estimated metallicity as low as $\leq \pm 0.2$ dex, i.e. close to the typical statistical uncertainty. In any case, a good safety criterion would be to limit the application to clusters older than 7−8 Gyr.

3. The sample of M 31 globular clusters

The M 31 GCs Lick indices used in this study are taken from our observations and from several sources available in literature. In this section we describe the various data we adopted and how we transformed the different sets of measures into the T98 system. In the following analysis we only consider objects classified

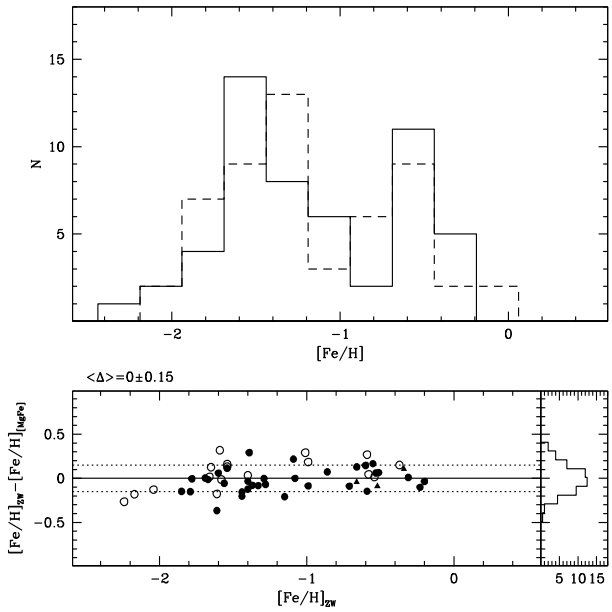

Fig. 4. *Upper panel*: comparison of the input MW GC metallicities from ZW84 and Armandroff & Zinn (1988) (continuous line) with those obtained from the empirical metallicity calibration (dashed line). *Lower panels*: comparison of the observed metallicity with the estimates from the [MgFe] index for Galactic GCs (T98: open circles; S05: filled circles; B04: triangles). The dashed lines enclose the rms.

in the RBC as *genuine old M 31 clusters*, i.e. having *classification flag* $f = 1$. The possibility of contaminating the sample by spurious sources is discussed in Sect. 3.4, below.

3.1. Indices from our own spectra

First, we obtained new measures of Lick indices for the sample of M 31 GCs described in Galleti et al. (2006a) and Galleti et al. (2007). The spectra were taken with the AF2/WYFFOS multi-fiber spectrograph at the 4.2 m William Herschel telescope (WHT), with DoLoRes at the 3.5 m Telescopio Nazionale Galileo (TNG), Roque de los Muchachos (La Palma, Spain), and with BFOSC at the Cassini 1.52 m telescope of the Loiano Observatory (Bologna, Italy). The data acquisition, reduction, and the resulting radial velocities (and membership) are fully described in Galleti et al. (2006a).

All the spectra were flux-calibrated, using various spectrophotometric standard stars to convert counts into flux units. We selected 88 confirmed clusters having the best spectra, i.e. $S/N \geq 15$, 69 from the WHT set, 14 from the TNG set, and 5 from the Loiano set. During each observing night we also collected accurate ($S/N > 20$) observations of GCs in common with T98.

All the selected spectra span a wavelength range including indices from Fe4531 to Fe5406. Each spectrum was shifted to zero radial velocity. Before measuring indices, one must carefully degrade spectra of higher resolution to the resolution of the Lick system. We strictly followed the approach of Worthey & Ottaviani (1997) and degraded our spectra to the wavelength-dependent Lick resolution (~11.5 Å at 4000 Å, 8.4 Å at 4900 Å, and 9.8 Å at 6000 Å) with a variable-width Gaussian kernel.

The derived indices were then compared with those provided by T98 for 9, 14, and 10 clusters in common for the WHT, Loiano, and TNG sets, respectively. It was found that all the considered indices can be reported in the T98 just by adding

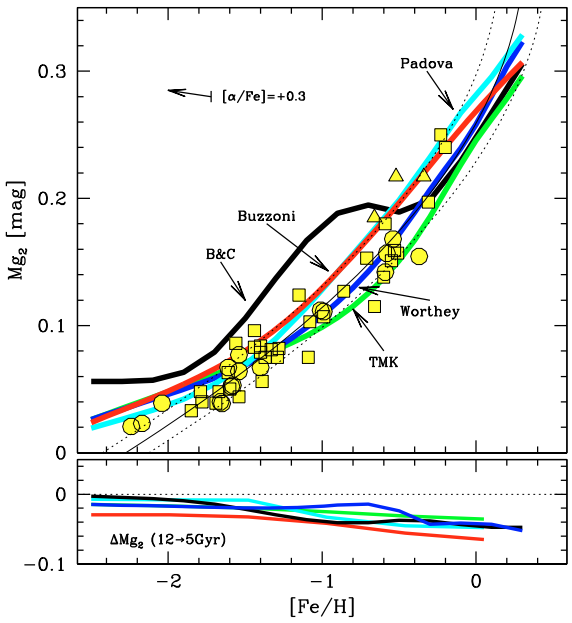

Fig. 5. *(upper panel)* – Mg2 index distribution of the MW GCs (symbols are the same as Fig. 3) compared to the stellar population models of Buzzoni (1989, 1995a), Worthey et al. (1994), Girardi et al. (2000) (labeled as "Padova" on the plot), Bruzual & Charlot (2003, "B&C"), Tantalo & Chiosi (2004b, "TMK"). An age of 12 Gyr is assumed throughout, with solar [α/Fe] element partition. The thin line indicates the empirical calibration with its 1σ uncertainty. The effect of α-element enhancement is sketched by the arrow, for a change [α/Fe] = +0.3. In *the lower panel* we assess the effect of a change in age. For the same theoretical models we report the expected index variation (Δ Mg$_2$) for a 5 Gyr stellar population along the full metallicity range. The color figure is available in the electronic edition.

Table 4. Correction terms of the transformation to match the Lick system for WHT, Loiano, and TNG data in the sense $I_{\rm Lick} = I_{\rm measured} + c$.

Index	c WHT	rms WHT	c Loi	rms Loi	c TNG	rms TNG
Mg2	0.015	0.022	0.018	0.015	–0.016	0.015
Mgb	0.000	0.588	–0.122	0.290	–0.333	0.399
Fe5270	–0.210	0.451	–0.148	0.504	–0.108	0.451
Fe5335	–0.230	0.346[a]	–0.188	0.287	–0.188	0.218

[a] We have not considered B178 in the fit for AF2/WYFFOS data.

the constant values listed in Table 4. The comparison between the *corrected* values from the various sets and the measures by T98 are shown in Fig. 6. Our Lick index measurements and index uncertainties are listed in Appendix A, Table A.1 (available in online edition). Errors were determined using photon statistics, following the formulae given in Cardiel et al. (1998). They do not incorporate the uncertainty due to our transformation to the Lick system, which is quantified by the rms scatter reported in Table 4.

3.2. Data from the literature

To assemble as large as possible a dataset of metallicities on the new scale, we complemented the measures described above with other clusters with published measures of the required Lick indices. In all cases we derived the equations to transform the published values into the T98 system using clusters in common

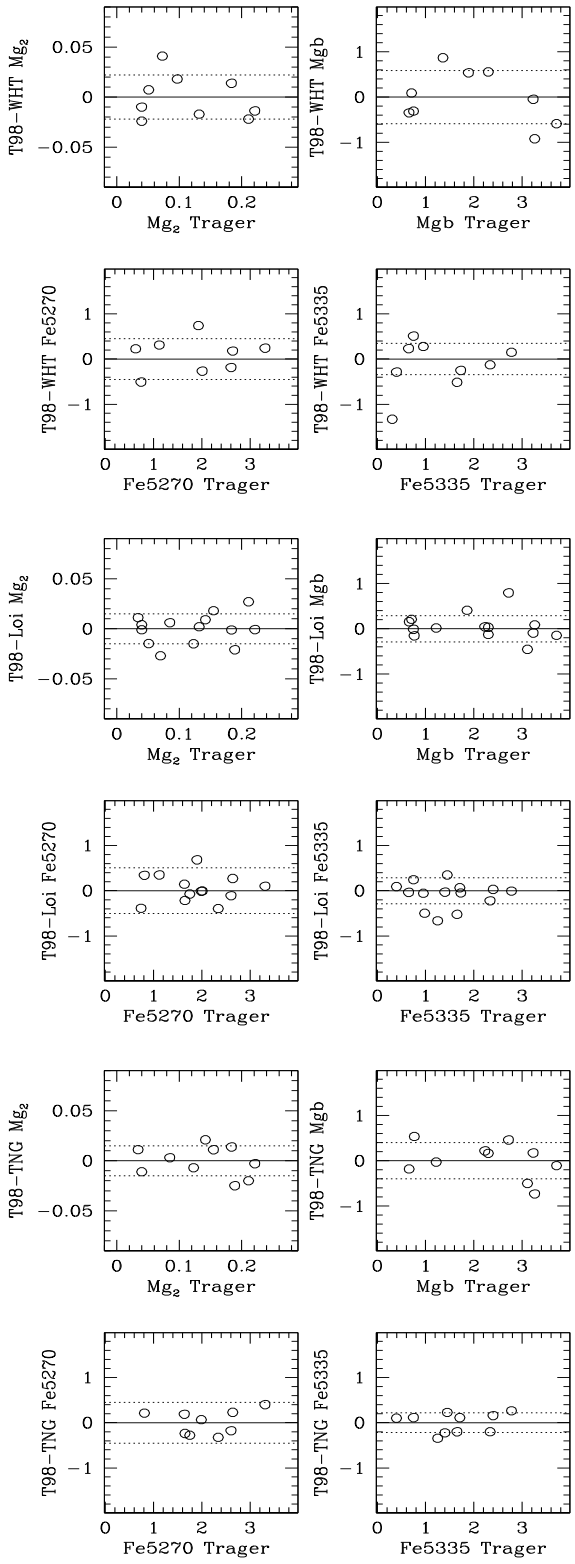

Fig. 6. Comparison of Lick indices measurements from WHT, Loiano, TNG after transformation and T98, for the clusters in common. The dotted lines enclose the range of the rms. In AF2/WYFFOS data for Fe5335 we have not considered B178 in the fit data. In Loiano and TNG data we have not considered B193.

between each considered set and T98, as done above for our measures. The following sources were adopted:

1. First, we included the measures by T98 itself, which are available for 18 M 31 GCs. These spectra were obtained by

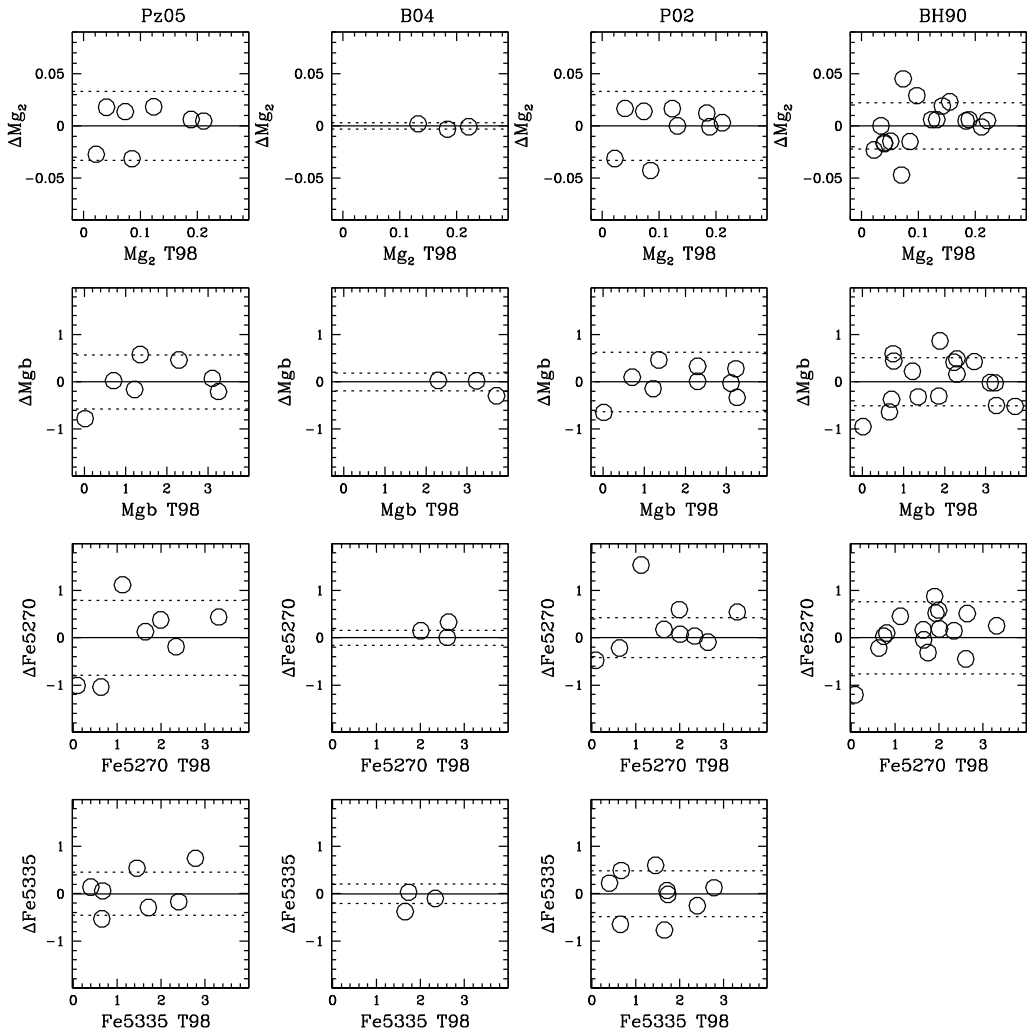

Fig. 7. Comparison of the literature metallicity indices transformed into the T98 system (according to Table 5) with T98 data. Dashed lines show the rms.

Burstein et al. (1984) with the image dissector scanner (IDS) at the 3 m Shane Telescope of the Lick Observatory. The absorption-line indices are re-measured by T98 system, and they define the standard system.

2. Indices for 30 clusters have taken from Beasley et al. (2004, B04), who obtained high S/N spectra ($S/N > 30$ pixel^{-1}) with the low-resolution imaging spectrograph (LRIS) on the Keck I telescope. The set of Lick line indices was measured with the passband definitions of Worthey et al. (1994) and was not corrected to the system of T98. However, the three clusters in common with T98 show excellent agreement with the standard system (see Fig. 7).
3. We incorporated the dataset of Puzia et al. (2005, Pz05), who measured Lick indices, with the T98 definition, for 29 M 31 GCs from the best spectra ($S/N > 25$ per Å) of the Perrett et al. (2002, hereafter P02) sample, obtained with the WYFFOS at the 4 m WHT telescope.
4. We also included the indices for a further ∼120 clusters, from the lower S/N spectra of the P02[4] sample. The absorption-line indices were measured with the old passband definitions of Faber (1973) and Brodie & Hanes (1986). When needed, we converted the value of P02 to the commonly used Å-scale for atomic indices[5].
5. The same procedure have applied to the Brodie & Huchra (1990, BH90) data obtained with the multiple mirror telescope (MMT). BH90 have measured ∼150 absorption-line indices in their bandpass definitions from atmospheric cut-off at 3200 Å to NaI, thus not including the Fe5335 index.

The various sets of indices (I_i) were transformed into the T98 system by the equation:

$$I_{\rm T98} = I_i + aI_i + c.$$

The coefficients of the adopted transformations are reported in Table 5, and the corrected indices are compared to the T98 values in Fig. 7. The same procedure was adopted to transform also

[4] Private communication.

[5] The transformation between wavelength and magnitude scale can be performed with the equations:

$$I_{\rm Å} = (\lambda_{\rm max} - \lambda_{\rm min})(1 - 10^{-0.4 I_{\rm m}}) \quad (3)$$

$$I_{\rm m} = -2.5 \log[1 - (I_{\rm Å}/(\lambda_{\rm max} - \lambda_{\rm min}))] \quad (4)$$

where $\lambda_{\rm max}$ and $\lambda_{\rm min}$ define the red and blue boundaries of the feature passband.

Table 5. Coefficient to transform the literature data (Pz05, B04, P02, and BH90) into the T98 system.

Index	*a*	*c*	rms	*a*	*c*	rms	*a*	*c*	rms	*a*	*c*	rms
	Pz05			B04			P02			BH90		
Mg2	0.731	0.017	0.033	0.000	–0.020	0.003	0.730	0.070	0.033	0.000	0.015	0.022
Mgb	0.764	0.424	0.572	0.000	0.000	0.186	0.681	0.240	0.631[a]	0.000	–0.27	0.508
Fe5270	0.000	0.000	0.790	0.000	0.000	0.161	0.000	–0.353	0.422[b]	0.639	0.731	0.762
Fe5335	0.000	0.000	0.454	0.000	0.000	0.208	0.000	0.000	0.485			

[a] We have not considered B015 in the fit data; [b] we have not considered B012 in the fit data.

the Hβ index into the T98 system, when available. In all the considered cases, a constant shift appears to be an adequate transformation. The comparison of the corrected Hβ values and the adopted shifts and rms are shown in Fig. 8.

3.3. Adopted metallicities

The indices transformed into the T98 system were used to compute the metallicities from Eqs. (1) and (2). In case of multiple measures of the same spectral index for a given GC, we always choose the value obtained from the spectrum with the highest S/N (when available) and/or with the smallest error. Individual indices estimates and the associated uncertainties for these datasets (296) are given in Appendix A, Table A.2 (available in online edition).

Cluster metallicities and the associated uncertainties were determined from Eq. (1) when possible, and from Mg2 in the other cases, i.e. when measures of Fe5270 and/or Fe5335 are lacking. Since the index-metallicity relation used is valid only for old GCs (see Sect. 2), we have removed all possibly young objects. The empirical metallicities for 245 M 31 GCs (see Sect. 3.4, below) are reported in Appendix A, Table A.3 (available in online edition).

3.4. Possible contaminations

All the M 31 clusters in our analysis are class $f = 1$ RBC entries; that is, they are all classified as genuine M 31 members whose nature has been confirmed either spectroscopically and/or by means of high-resolution imaging (see Galleti et al. 2006a, for a detailed discussion about the classification of M 31 GCs). While the sample should be largely dominated by bona-fide clusters, some spurious object may always be present as a truly final word on the nature of these objects can be obtained only by resolving them (at least partially) into individual stars by means of high-resolution imaging. However, the recently published broad spectroscopic and imaging survey by Caldwell et al. (2009) allows us to extensively check the classifications adopted in the RBC with fully independent and homogeneous data.

Of the 252 class $f = 1$ clusters that we originally considered in our analysis, 247 were also observed and classified by Caldwell et al. (2009), and only *seven* of them, namely B025D, B026D, B043D, B046D, B215D, B248D, and DAO25, were classified as non-clusters by these authors. For this reason, they were excluded from our sample, reducing the total number of clusters with metallicity estimate from 252 to 245. Moreover, both B289D and B292D are suspected by Caldwell et al. (2009) to in fact be stars. Since these cases are not clear-cut, we mark these objects as potentially misclassified but we keep them in our GC sample. Caldwell et al. (2009) *confirmed the RBC classification for all the remaining 238 clusters in common between the two samples*; i.e., all of them are classified as genuine globulars.

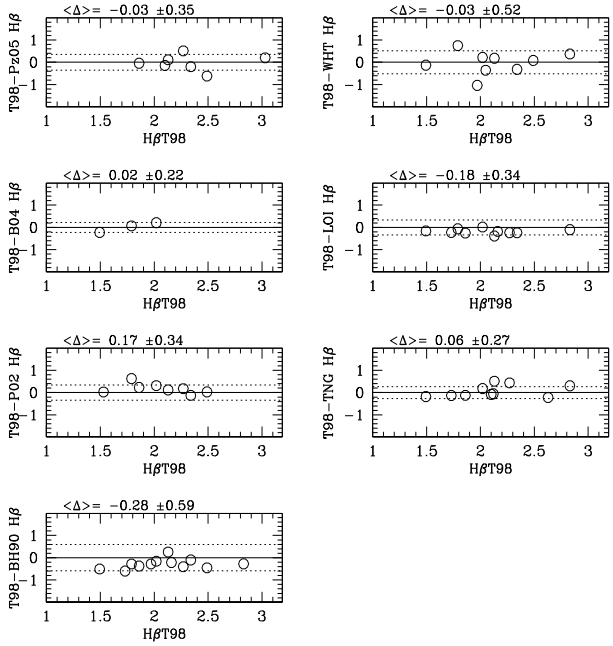

Fig. 8. Comparison of the Hβ index measurements with T98 values. The mean differences and rms are also reported. The dashed lines enclose the rms.

We stress that for the large majority of these clusters this classification has been previously confirmed also by other authors. Finally, of the five clusters of our sample that have not been observed by Caldwell et al. (2009), i.e. B514, MCGC1, MCGC8, MCGC10, and B344D, the first four have been confirmed as genuine old globulars from their HST CMDs (Galleti et al. 2006b; Mackey et al. 2007). According to the above cross-check, therefore, we conclude that, before the exclusion of the seven objects re-classified by Caldwell et al. (2009), the contamination of our sample by non-clusters was $\lesssim$4%, and should be significantly lower than this in the final, cleaned sample.

As said in the Sect. 2.1, the derived calibrations are only valid for old GCs (age > 7 Gyr), so it would be wise to exclude possibly young clusters from the final sample. The most widely used age indicators among Lick indices are the Balmer lines (see Fusi Pecci et al. 2005; Caldwell et al. 2009, and references therein). Here we adopt the Hβ index to clean our sample of possibly young objects on an objective basis. In particular, we have excluded all the objects with Hβ > 3.7 Å since the beginning (see Fusi Pecci et al. 2005, for a detailed discussion)[6].

[6] In Fusi Pecci et al. (2005), to select clusters (possibly) younger than 2 Gyr the selection criteria Hβ > 3.5 Å was adopted, using Hβ estimates from P02. However in the T98 system adopted here H$\beta_{\rm T98}$ = H$\beta_{\rm P02}$ + 0.17 Å (Fig. 8), hence the limit has been changed accordingly.

To investigate the problem in more detail, we checked any other cluster that has been suggested by some author as possibly young, irrespective of its Hβ value. Of 245 clusters for which we have derived metallicities, there are 28 such clusters (see Fusi Pecci et al. 2005). Seven of these have published color−magnitude diagrams showing that they are very likely old GCs: B311, B358, and B468 by Rich et al. (2005), B008 by Perina et al. (2009a), B083, B347, and NB16 by Perina et al. (2009b). An additional 16 clusters have been recently classified as old from their spectra by Caldwell et al. (2009, included in the cross-check described above), B015, B030, B047, B060, B070, B090, B117, B146, B154, B164, B197, B214, B232, B292, B328, B486. We did not find any additional information for the remaining five (B018, B316, B431, B240D, DAO30): conservatively, we maintain them in the list of clusters for which we provide a metallicity estimate, but we exclude them from the cleaned sample used in the following analysis (Sect. 5).

In conclusion, the degree of contamination from any kind of spurious object (non-cluster or young cluster) in the sample considered in Sect. 5 should be extremely low. It should be recalled that the adopted selection in Hβ would not exclude from our sample intermediate-age clusters (2 Gyr $\lesssim$ age $\lesssim$ 7 Gyr) that may be included with a wrong metallicity (lower than the true value). However, these clusters should be quite rare in M 31, if any, as among the several tens of M 31 clusters having a CMD from HST, none has been found in that age range.

4. Comparisons with other sets of metallicities

In the following sections we compare our metallicity estimates for M 31 GCs with those already available in the literature. We separately discuss the comparison with (a) estimates obtained from empirical calibrations of spectral indices or colors; (b) estimates obtained from the fit of observed spectra with theoretical SPSS models; and (c) estimates obtained from the analysis of the CMDs of individual clusters (see Fusi Pecci et al. 1996; Holland et al. 1997; Jablonka et al. 2000; Brown et al. 2004; Rich et al. 2005; Mackey et al. 2007; Perina et al. 2009a, and references therein).

4.1. Comparison with [Fe/H] from empirical calibrations

Before proceeding with the comparison of our new scale with previous analysis, it is worth having a look at the degree of consistency between already existing sets. The comparison between H91 and P02 is particularly relevant in this context, because (a) they are the largest sets of empirical metallicities for M 31 GCs available in the literature; (b) they should be consistent *by definition*, because P02 uses the same definitions of the indices as H91 (see Brodie & Huchra 1990, hereafter BH90), and uses metallicities by H91 for clusters in common between the two sets to calibrate [Fe/H] vs. indices. To the original set of H91 we added the metallicities for further 35 M 31 GCs obtained by Barmby et al. (2000) with the same method and strictly in the same system as H91.

The left panel of Fig. 9 reveals that there is considerable scatter between the H91 and P02 sets of measures: the rms is 0.34 dex but differences up to ∼1 dex are also present. This can be taken as a reference of the typical degree of agreement between independent sets. In the right panel we compare the P02 metallicities with those Pz05 where the dataset is the same. A wide spread is also evident in this case.

It is important to recall here that to obtain the metallicity of M 31 GCs from line indices, BH90 and H91 calibrated a relation

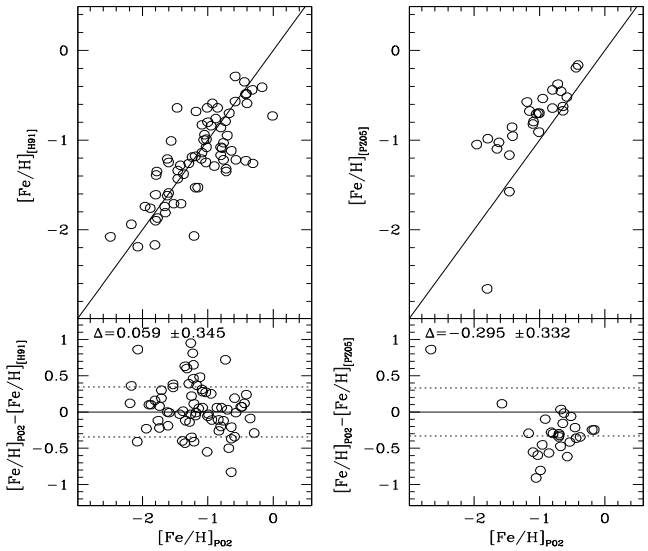

Fig. 9. Comparison of the metallicities from P02 with H91 and B00 in *the left panel* and from P02 with Pz05 in *the right panel*. The solid line indicates the one-to-one relation. The dotted lines in *the lower panel* mark the σ value.

between [Fe/H] and the infrared colors ($(V-K)$, $(J-K)$) using Galactic GCs. Then, they used the infrared photometry of 40 M 31 GCs by Frogel et al. (1980) and Bonoli et al. (1987) to obtain their metallicity from that relation, and merged this sample with i) a sample of Galactic GCs for which they measured the same line indices and ii) with the average of the indices measured in several individual stars in the open cluster NGC 188, which was adopted as a template for solar metallicity populations lacking among MW globulars. They used the merged sample to calibrate various indices against [Fe/H]. Finally, they used the relations to obtain a metallicity estimate for each index, and they adopted the weighted average of the values obtained from the various indices as their final metallicity estimate (H91). The complex procedure outlined above was dictated by the requirement to obtain the largest possible sample from the data available at the time and to average out the errors by using the information from all the available indicators. On the other hand, our aim is to provide a clean and easily repeatable process to obtain metallicities from few selected spectral indices, because nowadays it is relatively easy to obtain high S/N spectra for most M 31 GCs with 4m telescopes, and the 10 m class telescopes are entering the game.

Figure 10 shows that the difference between our metallicity estimates and those from H91 and P02 presents a scatter of the same amplitude as that existing between H91 and P02. Moreover, metallicities from our scale are systematically higher by up to ∼0.3 dex for [Fe/H] $\gtrsim -1.4$ and systematically lower for [Fe/H] $\lesssim -2.0$. Figure 10 provides a strong warning on the reliability of empirical metallicity scales based on Lick indices from integrated spectra. While our metallicities and those by H91 and P02 present strong correlations, estimates for individual clusters can differ by as much as ±0.5 dex (or more) because of statistic or systematic effects. This is the fundamental reason for avoiding assembling metallicities from different sources for the RBC, trying instead to reach the maximum degree of homogeneity at the "index level" (Sects. 2 and 3) and the highest degree of internal consistency by converting the indices into metallicity with the same calibrating relations. The choice of using just the Mg2, Mgb, Fe5270, and Fe5335 indices

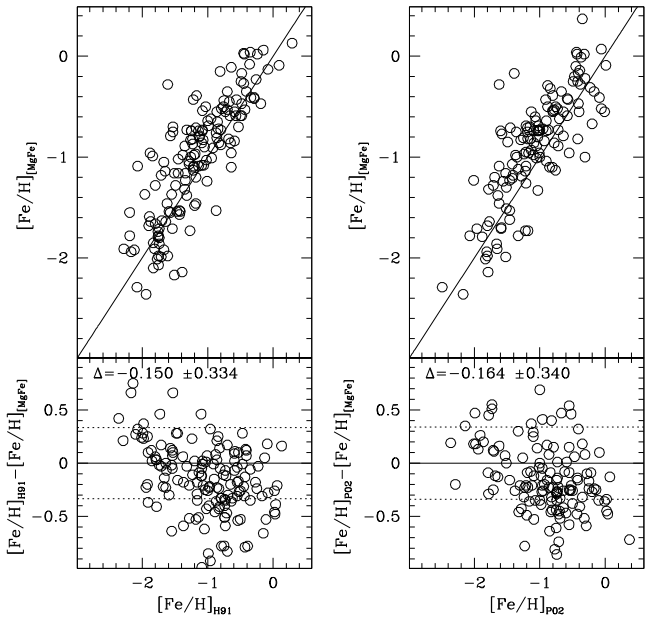

Fig. 10. Comparison of our empirical metallicities of M 31 GCs with P02 and H91. The solid line indicates the one-to-one relation. The dotted lines in *the lower panel* enclose the rms. Error bars have been omitted in the panels for clarity.

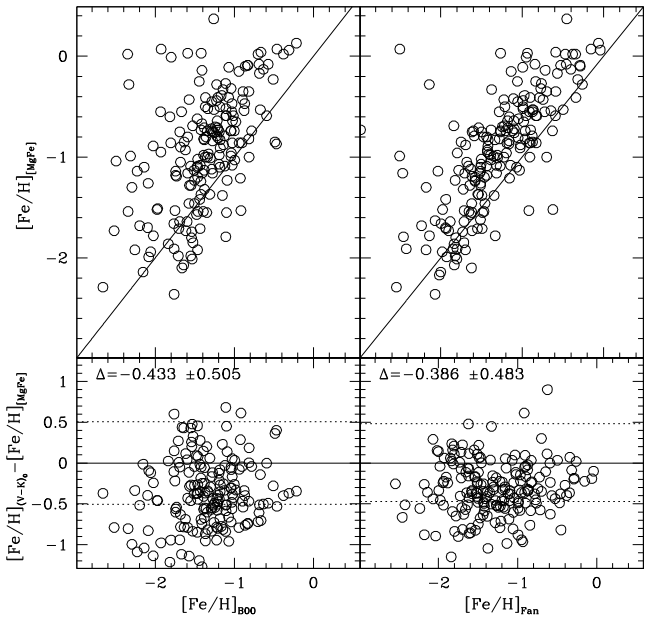

Fig. 11. Comparison of our empirical metallicities of M 31 GCs with those obtained from $(V-K)_0$, using the calibrations by Barmby et al. (2000) and adopting two different sets of reddening estimates: Barmby et al. (2000) (*left*) and Fan et al. (2008) (*right*). The solid line indicates the one-to-one relation; in *the lower panels*, the dotted lines enclose the rms.

is also intended to minimize the effects on the final metallicity estimate of variations/anomalies in the abundance of other elements, such as C, N, or age effects, that may affect other indices (see, for example, Burstein et al. 2004; Fusi Pecci et al. 2005, and references therein). It is worth noting, in this context, that we have no particular a-posteriori reason to claim that our scale is *superior* to other existing empirical scales based on spectra. We feel that we have made all possible effort to construct a very homogeneous and internally consistent scale for the RBC, designed for the easy and safe inclusion of any new set of indices that will be published in the future[7].

Finally, Fig. 11 shows the comparison between our metallicities and those obtained from $(V-K)_0$ colors, using the calibrations by Barmby et al. (2000), taking the $V-K$ colors from the RBC, and adopting two different sets of reddening estimates, i.e. those from Barmby et al. (2000)[8] and from Fan et al. (2008). This comparison reveals the critical role of the (uncertain) reddening estimates on any metallicity scale based on colors: the two sets considered here differ only in the adopted reddening, yet the rms scatter in the final metallicity is as high as ±0.30 dex. The overall behavior in comparison with our scale is relatively similar to that of the H91 and P02 sets. This may stem from the origin of these scales also being a calibration of metallicity vs. integrated $(V-K)_0$ colors.

It is interesting to note that, independent of the adopted set of reddening, the metallicities obtained from $(V-K)_0$ are systematically lower than our spectroscopic estimates by a large amount, i.e. ≃0.4 dex, on average. We do not have any straightforward explanation for this remarkable systematic difference, we can just put forward some hypothesis for its origin. The observed effect can arise if the reddening values are systematically overestimated: using the [Fe/H] − $(V-K)_0$ calibration by Barmby et al. (2000) and assuming $E(V-K) = 2.75E(B-V)$, according to Cardelli et al. (1989), an overestimate of $E(B-V)$ by 0.09, on average, is enough to account for the whole 0.4 dex difference between the metallicity scales. While the required systematic in $E(B-V)$ is probably too large to be realistic, an overestimate of the reddening may provide a relevant (possibly the largest) contribution to the observed systematic difference in the metallicity. Systematic differences in the age distribution and/or in the abundance pattern between MW and M 31 globulars can also contribute to the effect. In particular, Fig. 9 of Barmby et al. (2000) seems to suggest that the clusters of the two galaxies may not share the same [Fe/H] − $(V-K)_0$ relation.

4.2. Comparison with [Fe/H] from SED fitting

We compare the metallicities of the M 31 clusters derived from our empirical calibrations with those derived from SSP model fitting by Puzia et al. (2005) and Beasley et al. (2005) (using the TMB models) in Fig. 12. The models report the metallicities in [Z/H] scale and a transformation to [Fe/H] has been done through the equation [Fe/H] = [Z/H] − 0.94[α/Fe] taken from Thomas et al. (2003; see also Trager et al. 2000). The clusters with derived age < 8 Gyr are excluded because our empirical calibrations are only valid for old GCs. To first order, the agreement between the literature values and the metallicities from our empirical relations is clearly satisfactory with B05, and acceptable with Pz05, as shown in Fig. 12. The two sets of measures show systematics of opposite signs with respect to our scale: B05 finds values slightly lower than ours (by ∼0.1 dex), Pz05 estimates are larger by ∼0.2 dex, on average. It may be worthwhile to check that part of these differences may be due to these authors considering the metallicity from iron peaks elements and the abundance

[7] This will be possible on condition that the considered set of indices have enough clusters in common with our sample to obtain a good transformation of the indices into the T98 system.

[8] Private communication.

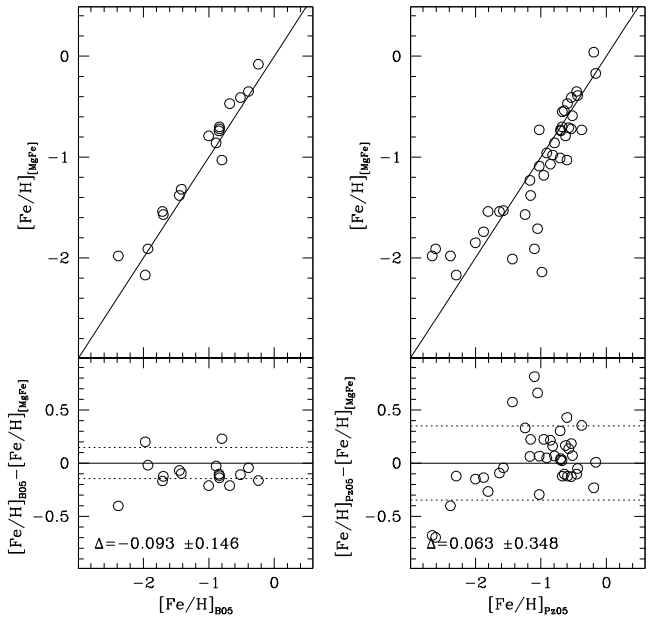

Fig. 12. M 31 clusters empirical metallicities vs. the [Fe/H] values derived by Puzia et al. (2005) (*left panel*) and Beasley et al. (2005) (*right panel*) from SSP model fitting (see text, Sect. 4.2).

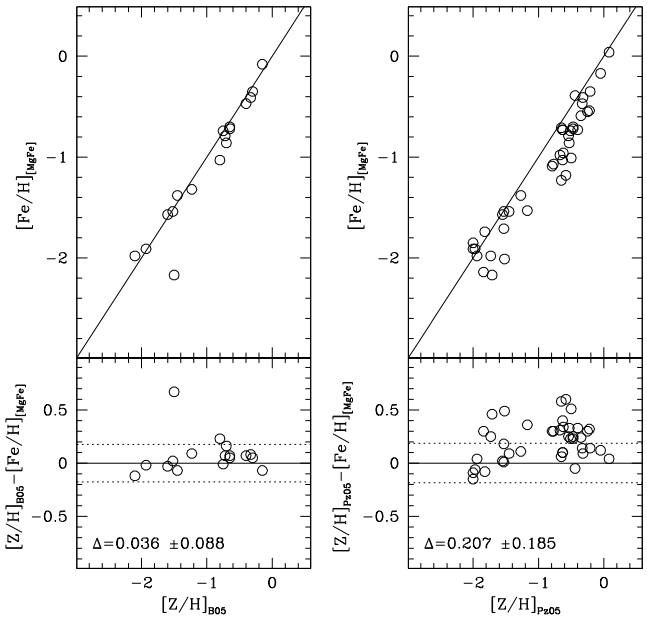

Fig. 13. The same as Fig. 12, but using [Z/H].

of α elements separately, while our scale neglects this potentially relevant discrimination[9].

Figure 13 shows that this may be the case for B05. If our [Fe/H] estimates are compared with B05 estimates of [Z/H], the offset is reduced to zero and even the rms scatter is slightly reduced (having excluded the outlier B328). On the other hand, the comparison with [Z/H] exacerbates the systematic difference with Pz05, while significantly reducing the rms scatter. In conclusion, our new metallicity scale seems in much better agreement with scales derived from the detailed fitting of spectra with SPSS models than with other empirical scales.

4.3. Comparison with [Fe/H] from CMDs

The estimates that can be obtained from CMDs of individual clusters by comparing the observed red giant branch (RGB) with the RGB templates of well-studied Galactic GCs probably provides one of the most reliable metallicities currently available for M 31 GCs, of course under the hypothesis that the basic properties of the two GC systems are the same. For clusters that are not too compact and are not immersed in exceedingly crowded fields, HST photometry (either from the WFPC2, e.g. Rich et al. 2005, or the ACS, e.g. see Galleti et al. 2006b; Mackey et al. 2007) can provide clean and well-defined CMDs of the RGB. In addition the horizontal branch morphology and the lack of bright main sequence stars give the best sanity check on the actual age of the cluster that can be currently achieved (see, in particular Brown et al. 2004). Therefore, the comparison of our estimates with those obtained from good CMDs from HST is a compelling test of the reliability and accuracy of our new metallicity scale.

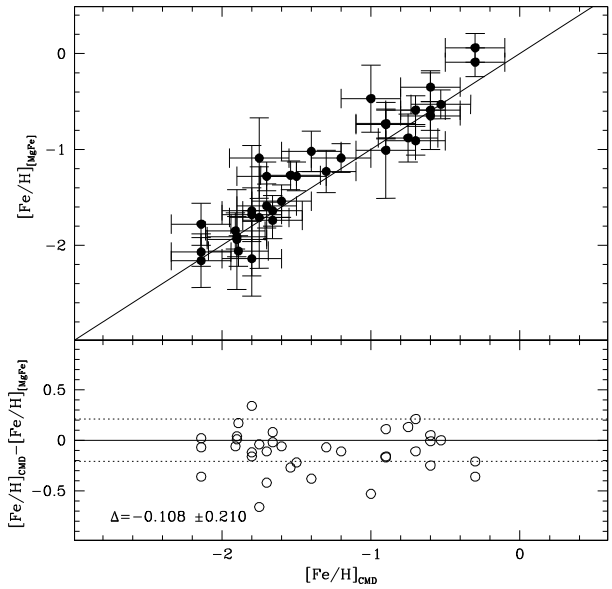

Fig. 14. [Fe/H] estimates from CMDs of individual clusters (from good quality HST photometry) compared with the metallicities derived in the present analysis. The mean offset ± the standard deviation are reported in *the lower panel*.

We collected metallicity from CMDs for 35 clusters in common with our list, from the following sources: Rich et al. (2005), the largest sample of published CMD of M 31 GCs; Jablonka et al. (2000), which analyzed three GC in the bulge of M 31; Brown et al. (2004), which studied B379 in great detail; Galleti et al. (2006b) and Mackey et al. (2007), which considered clusters located in the outskirts of the galaxy and Perina et al. (2009a). The comparison between our estimates and those obtained from the CMDs is presented in Fig. 14. The agreement is quite satisfying over the whole considered range. However, there is a small systematic offset between the metallicity estimates obtained from the spectra or from the CMDs, in the sense that the former are higher than the latter by ∼0.1 dex, on average. This points to a real difference between the two independent

[9] It is important to recall that our scale is not expected to strictly trace the abundance of *iron*. In fact, it is based on the ZW84 scale that, in turn, is based on the metallicities derived by Cohen (1983) from lines of various elements, including Mg (see Mendel et al. 2007, for a detailed discussion and references). Therefore it is likely a better proxy for the *total* metallicity than for the actual iron abundance.

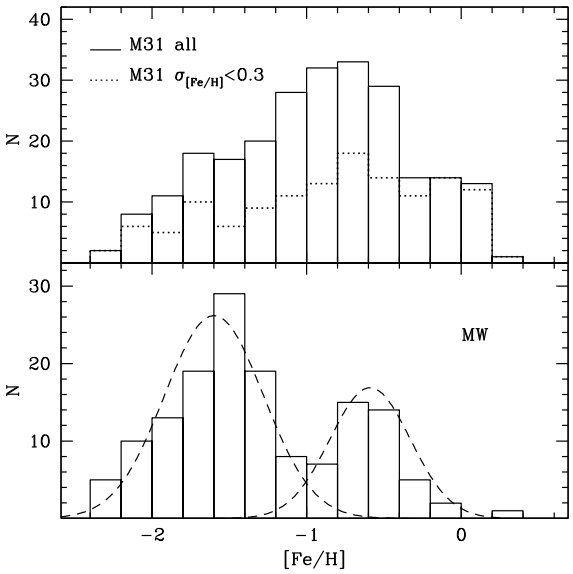

Fig. 15. Metallicity histograms for the M 31 (*top*) and the MW (*bottom*) GC systems. Dashed lines in the lower plot are the Gaussian curves in the best-fit model as found by the KMM algorithm for two subpopulations (Fe/H] = −1.60 and −0.59 dex).

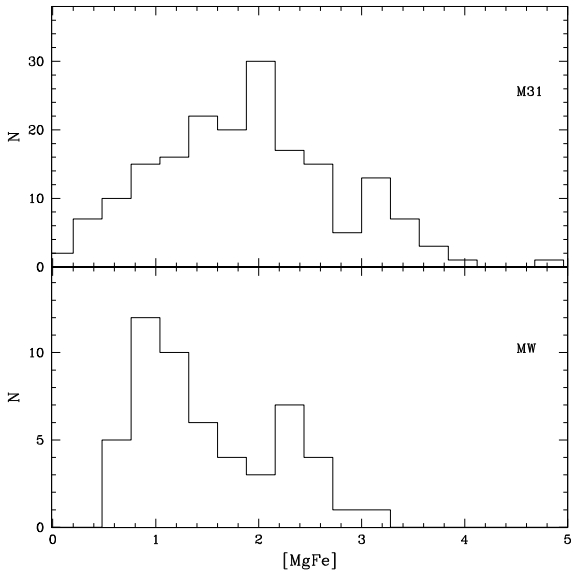

Fig. 16. [MgFe] distribution for M 31 GCs (*upper panel*) and the MW GCs (*lower panel*).

scales, possibly related to how [α/Fe] is included in the two calibrations. We take the rms of the difference computed over the whole sample as the typical accuracy of our metallicity estimates (±0.25 dex).

5. Discussion and conclusions

Using our own data, as well as datasets available in the literature, we have established a new homogeneous metallicity scale for M 31 GCs. The scale is based on the Lick index Mg2 and on the combination of Mgb and Fe indices [MgFe] that have been calibrated against well-studied Galactic globulars (for [Fe/H] < −0.2) and a variety of SSP theoretical models for −0.2 ≤ [Fe/H] ≤ 0.50 and age ∼ 12 Gyr. Our scale has been shown to be self-consistent within ±0.25 dex, and it should only be applied to classical, old GCs.

In the following we briefly describe a few natural applications of the newly derived metallicity scale. In particular, (a) we derive and discuss the metallicity distribution of M 31 GCs; and (b) we explore the correlations between metallicity and kinematics, for the sample of 240 bona-fide old GCs described in Sect. 3.4, above.

5.1. Metallicity distribution

In Fig. 15 the metallicity distribution (MD) of our sample of M 31 GCs is compared with its MW counterpart. The highest peak in the M 31 MD occurs at [Fe/H] ∼ −0.9, coinciding with the overall average of the sample ⟨[Fe/H]⟩ = −0.94, significantly more metal rich than in the MW case, where the maximum is at [Fe/H] ∼ −1.5 and the overall mean is ⟨[Fe/H]⟩ = −1.30 (based on data from Harris 1996, that are in the ZW84 scale). The M 31 system appears also to have a much larger fraction of clusters having [Fe/H] > −0.5 (23% of the total sample) with respect to the MW (7%). It should be considered that the individual metallicity estimates for M 31 clusters have much larger uncertainties with respect to their MW counterparts and this may produce some spurious widening of the MD for M 31. However, the shape of the distribution is essentially unchanged if we limit the analysis to the subset of clusters having errors in metallicity lower than ±0.3 dex (132 clusters; dotted histogram in the upper panel of Fig. 15). Figure 16 shows that the difference between the MDs of the two galaxies cannot be ascribed to spurious effects due to our calibration, as it can be re-conduced to genuine differences in the observable [MgFe].

The MD of M 31 GCs do not present any obvious structure like the bimodality encountered in the GC system of the MW. Nevertheless the distribution for M 31 clusters does not seem to be well represented by a single Gaussian distribution. Large errors on individual metallicities should contribute to wiping out real structures, not to producing spurious ones. The hypothesis of a multimodal underlying distribution has been compared with a unimodal representation using the parametric KMM test (Ashman et al. 1994), which compares the fits to the MD made with one or more Gaussian distributions. A two-component model with modes at [Fe/H] = −1.54 and [Fe/H] = −0.64 is preferred to the unimodal case at the 99.1% confidence level (homoscedastic case) and at the 98.7% c.l. in the heteroscedastic case with peaks at [Fe/H] = −1.79 and [Fe/H] = −0.76. A three-component model with modes at [Fe/H] = −0.25, −0.89, and −1.72 is also preferable to the unimodal one (99.8% c.l., in the homoscedastic case, and 99.6% c.l., in the heteroscedastic case with peaks at [Fe/H] = −1.77, [Fe/H] = −0.80 and [Fe/H] = −0.01), and nearly equivalent to the bimodal representation, from a statistical point of view. The preference of bi- and three- modal models over the unimodal case remains even if we consider the subset of clusters with the lowest metallicity errors described above. While clearly not conclusive, the above analysis suggests that there may be actual structures in the MD of M 31 GCs, in close agreement with the conclusions reached by Barmby et al. (2000), P02, Pz05, Fan et al. (2008) and Lee et al. (2008).

5.2. Metallicity and kinematics

Figure 17 shows the positional and kinematical properties of M 31 GCs divided into three groups according to their metallicity, i.e. a metal poor (MP) group ([Fe/H] ≤ −1.0), a metal

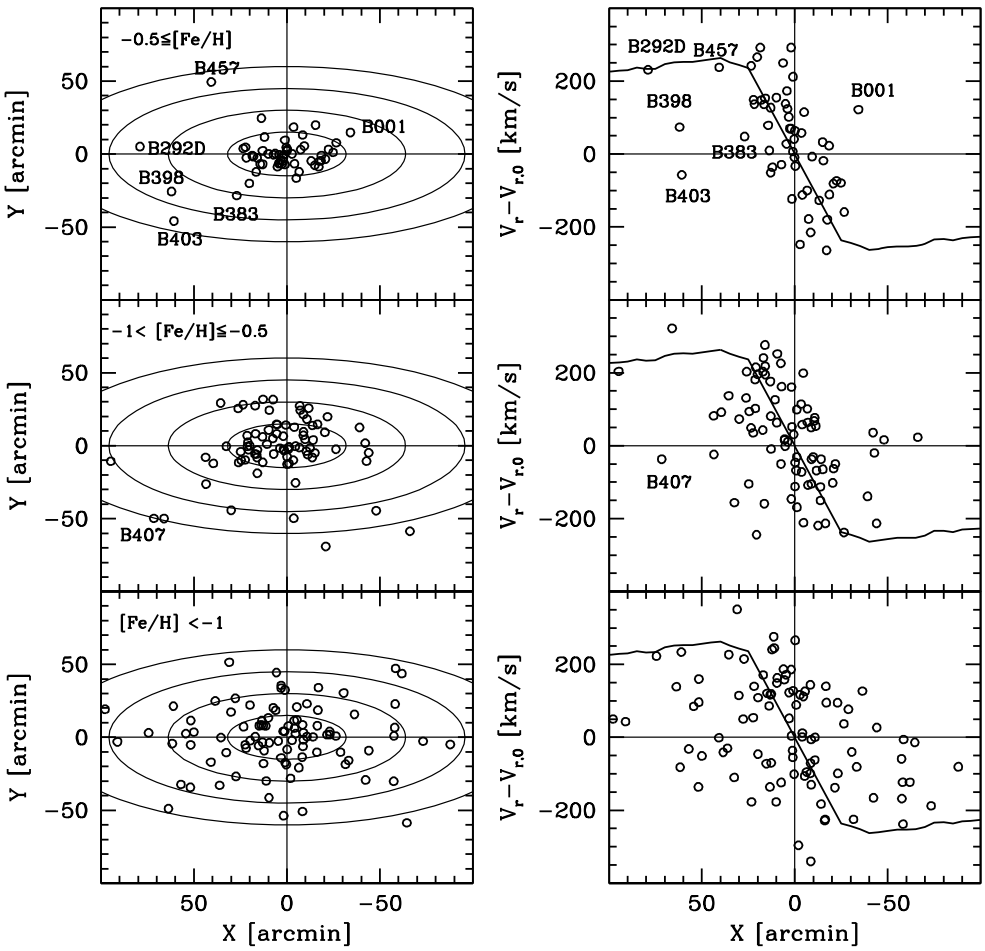

Fig. 17. *Left panels*: spatial distribution of three metallicity groups GCs in M 31. The ellipses have a semimajor axis of 15, 30, 45, 60 arcmin. *Right panels*: radial velocities vs. the projected distances along the major axis (X). The solid line shows an HI rotation curve from Carignan et al. (2006).

intermediate (MI) group ($-1.0 < [\mathrm{Fe/H}] < -0.5$), and a metal rich (MR) group ($[\mathrm{Fe/H}] \geq -0.5$). The left panels of Fig. 17 show the spatial distribution of the considered clusters in the canonical X, Y projected coordinate system (see Galleti et al. 2004, and references therein), with X along the major axis of the galaxy. In the right panels the radial velocity of the clusters (in the reference frame of M 31) is plotted versus the X coordinate and compared with the rotation curve of the HI disk from Carignan et al. (2006).

It is quite clear from the inspection of Fig. 17 that the MR and MI subsamples display a significant rotation pattern, similar to the rotation curve of neutral hydrogen disk of M 31. The MR clusters are more densely packed near the center of the galaxy and appear to follow the HI curve more closely, whereas the MI clusters display a larger dispersion. MR clusters are likely associated with the prominent bulge of M 31.

The MP clusters show a much larger velocity dispersion at any distance from the center of the galaxy; in spite of that, they follow a significant rotation pattern in the same sense as the other clusters. Dividing the MP sample at $X = 0$, we find (M 31-centric) average velocities of $\langle V_{\mathrm{M\,31}} \rangle = +59$ km s^{-1} and $\langle V_{\mathrm{M\,31}} \rangle = -48$ km s^{-1} for the clusters with $X > 0$ and $X < 0$, respectively; the difference in the median velocities is even greater, as $V^{\mathrm{med}}_{\mathrm{M\,31}} = +86$ km s^{-1} and $V^{\mathrm{med}}_{\mathrm{M\,31}} = -59$ km s^{-1}, for the two subsets. Finally if the $V_{M\,31}$ distributions of the $X > 0$ and $X < 0$ MP clusters are compared with a Kolmogorov-Smirnov test, it turns out that the probability that the two samples are drawn from the same distribution of $V_{\mathrm{M\,31}}$ is just 0.2%. In Sect. 3.4 we have shown that our sample should be reasonably clean from spurious sources (as for instance young massive clusters, which could be misclassified as metal-poor GCs and would follow the rotation pattern of the thin disk they belong to, see Fusi Pecci et al. 2005), so we conclude that the rotation pattern of MP clusters is probably real. However, an ultimate conclusion on this (relevant) issue could only be achieved when the actual nature of a significant subsample of MP clusters had been confirmed beyond any doubt from the CMD of their individual stars.

The above results agree with what was previously found by P02 and Lee et al. (2008), among others. A more detailed discussion of these correlations between kinematics and metallicity is beyond the scope of the present paper, but we address the interested reader to the thorough discussion by Lee et al. (2008). Here we simply want to draw attention on five of the six MR clusters lying at $R > 30'$ (labeled in Fig. 17). B001, B398, and B403 show no correlation with the overall rotation pattern. On the other hand, B292D, and B457 lie straight on the flat branch of the HI rotation curve in spite of being more than ∼7 kpc away from all the other MR clusters (except B398 and B403, of course). These five objects clearly deserve new observations with high S/N spectra to verify both their metallicity and their radial velocity. If confirmed, their odd positions and kinematics would require an interpretation. Moreover,

B403 and B407 (labeled in the MI panel of Fig. 17, and having [Fe/H] = −0.65 ± 0.15) have very similar position and velocity (differing by ∼20 km s^{-1}). The case of these two relatively metal-rich clusters in the outer halo of M 31 is discussed in more detail in Perina et al. (2009a)[10].

Acknowledgements. M.B. acknowledge the financial support of INAF through the PRIN2007 grant CRA 1.06.10.04. We are very grateful to P. Barmby and K. Perrett for providing their unpublished data for M 31 GCs. This research has made use of NASA's Astrophysics Data System Bibliographic Services. We would like to thank the anonymous referee for his/her careful reading of the manuscript and helpful comments.

References

Armandroff, T. E., & Zinn, R. 1988, AJ, 96, 92
Ashman, K. M., Bird, C. M., & Zepf, S. E. 1994, AJ, 108, 2348
Barmby, P., Huchra, J. P., Brodie, J. P., et al. 2000, AJ, 119, 727 [B00]
Beasley, M. A., Brodie, J. P., Strader, J., et al. 2004, AJ, 128, 1623 [B04]
Beasley, M. A., Brodie, J. P., Strader, J., et al. 2005, AJ, 129, 1412
Bonoli, F., Delpino, F., Federici, L., & Fusi Pecci, F. 1987, A&A, 185, 25
Brodie, J. P., & Hanes, D. A. 1986, ApJ, 300, 258
Brodie, J. P., & Huchra, J. P. 1990, ApJ, 362, 503 [BH90]
Brodie, J. P., & Huchra, J. P. 1991, ApJ, 379, 157
Brodie, J. P., & Strader, J. 2006, ARA&A, 44, 193
Brown, T. M., Ferguson, H. C., Smith, E., et al. 2004, ApJ, 613, L125
Bruzual, G., & Charlot, S. 2003, MNRAS, 344, 1000 [BC03]
Burstein, D., Faber, S. M., Gaskell, C. M., & Krumm, N. 1984, ApJ, 287, 586
Burstein, D., Li, Y., Freeman, K. C., et al. 2004, ApJ, 614, 158
Buzzoni A. 1989, ApJS, 71, 817 (see also: http://www.bo.astro.it/~eps/home.html for the latest model update)
Buzzoni, A. 1995a, ApJS, 98, 69
Buzzoni, A. 1995b in Fresh views of elliptical galaxies, ed. A. Buzzoni, A. Renzini, & A. Serrano (San Francisco: ASP), ASP Conf. Ser., 86, 189
Buzzoni, A., Gariboldi, G., & Mantegazza, L. 1992, AJ, 103, 1814
Buzzoni, A., Mantegazza, L., & Gariboldi, G. 1994, AJ, 107, 513
Caldwell, N., Caldwell, N., Harding, P., et al. 2009, AJ, 137, 94
Cardelli, J. A., Clayton, G. C., & Mathis, J. S. 1989, ApJ, 345, 245
Cardiel, N., Gorgas, J., Cenarro, J., & Gonzalez, J. J. 1998, A&AS, 127, 597
Carignan, C., Chemin, L., Huchtmeier, W. K., et al. 2006, ApJ, 641, L109
Carretta, E., & Gratton, R. G. 1997, A&AS, 121, 95
Carretta, E., Bragaglia, A., Gratton, R., & Lucatello, S. 2008, in Chemical Evolution of Dwarf Galaxies and Stellar Clusters [arXiv:0811.3591]
Cohen, J. G. 1983, ApJ, 270, 654
Cohen, J. G., Blakeslee, J. P., & Ryzhov, A. 1998, ApJ, 496, 808
Cohen, J. G., Blakeslee, J. P., & Côté, P. 2003, ApJ, 592, 866
Colucci, J. E., Bernstein, R. A., Cameron, S., et al. 2009, ApJ, 704, 385
Faber, S. M. 1973, ApJ, 179, 731
Faber, S. M., Friel, E. D., Burstein, D., & Gaskell, C. M. 1985, ApJS, 57, 711
Fan, Z., Ma, J., de Grijs, R., & Zhou, X. 2008, MNRAS, 385, 1973
Frogel, J. A., Persson, S. E., & Cohen, J. G. 1980, ApJ, 240, 785
Fusi Pecci, F., Buonanno, R., Cacciari, C., et al. 1996, AJ, 112, 1461
Fusi Pecci, F., Bellazzini, M., Buzzoni, A., et al. 2005, AJ, 130, 554
Galleti, S., Federici, L., Bellazzini, M., et al. 2004, A&A, 416, 917
Galleti, S., Federici, L., Bellazzini, M., et al. 2006a, A&A, 456, 985
Galleti, S., Federici, L., Bellazzini, M., et al. 2006b, ApJ, 650, L107
Galleti, S., Bellazzini, M., Federici, L., et al. 2007, A&A, 471, 127
Girardi, L., Bressan, A., Bertelli, G., & Chiosi, C. 2000, A&A, 354, 892
González, J. J. 1993, Ph.D. Thesis
Gratton, R. G., Fusi Pecci, F., Carretta, E., et al. 1997, ApJ, 491, 749
Gratton, R., Sneden, C., & Carretta, E. 2004, ARA&A, 42, 385
Harris, G. L. H., Geisler, D., Harris, H. C., & Hesser, J. E. 1992, AJ, 104, 613
Harris, W. E. 1996, AJ, 112, 1487 (see also: http://physwww.physics.mcmaster.ca/~harris/mwgc.dat for catalog update February 2003)
Holland, S., Fahlman, G. G., & Richer, H. B. 1997, AJ, 114, 1488
Huchra, J. P., Brodie, J. P., & Kent, S. 1991, ApJ, 370, 495 [H91]
Ibata, R., Martin, N. F., Irwin, M. J., et al. 2007, ApJ, 671, 1591
Isobe, T., Feigelson, E. D., Akritas, M. G., & Babu, G. J. 1990, ApJ, 364, 104
Jablonka, P., Courbin, F., Meylan, G., et al. 2000, A&A, 359, 131
Lee, M. G., Hwang, H. S., Kim, S. C., et al. 2008, ApJ, 674, 886
MacArthur, L. A. 2005, ApJ, 623, 795
Mackey, A. D., Huxor, A., Ferguson, A. M. N., et al. 2007, ApJ, 655, L85
Mackey, A. D., Ferguson, A. M. N., Irwin, M. J., et al. 2009, MNRAS, in press [arXiv:0909.1456]
McWilliam, A. 1997, ARA&A, 35, 503
Mendel, J. T., Proctor, R. N., & Forbes, D. A. 2007, MNRAS, 379, 1618
Perrett, K. M., Bridges, T. J., Hanes, D. A., et al. 2002, AJ, 123, 2490 [P02]
Perina, S., Federici, L., Bellazzini, M., et al. 2009a, A&A, 507, 1375
Perina, S., Cohen, J. G., Barmby, P., et al. 2009b, A&A, accepted [arXiv:0911.3166]
Press, W. H., Teukolsky, S. A., Vettering, W. T., & Flannery, B. B. 1992, Numerical Recipes in FORTRAN, Second edition
Pritzl, B. J., Venn, K. A., & Irwin, M. 2005, AJ, 130, 2140
Puzia, T. H., Perrett, K. M., & Bridges, T. J. 2005, A&A, 434, 909 [Pz05]
Renzini, A., & Fusi Pecci, F. 1988, ARA&A, 26, 199 [RFP88]
Renzini, A., & Buzzoni, A. 1986, in Spectral evolution of galaxies (Dordrecht: D. Reidel Publishing Co.), 195
Rich, R. M., Corsi, C. E., Cacciari, C., et al. 2005, AJ, 129, 2670
Schiavon, R. P., Rose, J. A., Courteau, S., et al. 2005, ApJS, 160, 163 [S05]
Schlegel, D. J., Finkbeiner, D. P., & Davis, M. 1998, ApJ, 500, 525
Sneden, C. 2005, IAU Symp., 228, 337
Tantalo, R., & Chiosi, C. 2004, MNRAS, 353, 405
Tantalo, R., & Chiosi, C. 2004, MNRAS, 353, 917
Thomas, D., Maraston, C., & Bender, R. 2003, MNRAS, 339, 897 [TMB]
Thomas, D., Maraston, C., & Korn, A. 2004, MNRAS, 351, 19
Trager, S. C., Worthey, G., Faber, S. M., et al. 1998, ApJS, 116, 1 [T98]
Trager, S. C., Faber, S. M., Worthey, G., & González, J. J. 2000, AJ, 119, 1645
van den Bergh, S. 1969, ApJS, 19, 145
Worthey, G. 1994, ApJS, 95, 107
Worthey, G. 1996, ASPC, 98, 467
Worthey, G., & Ottaviani, D. L. 1997, ApJS, 111, 377
Worthey, G., Faber, S. M., Gonzalez, J. J., & Burstein, D. 1994, ApJS, 94, 687
Zinn, R. 1985, ApJ, 293, 424
Zinn, R., & West, M. J. 1984, ApJS, 55, 45 [ZW84]

[10] *Note Added in Proofs*: after the acceptance of the present paper, a work appeared presenting metallicities of a few M 31 GCs from high resolution integrated spectra (Colucci et al. 2009). It is interesting to note that for four of the five clusters in common, our [Fe/H] estimates agree with those of Colucci et al. (2009) to within <0.1 dex. Our estimate for the fifth cluster (B358, which is in the deep metal-poor regime in which our observables are less sensitive to metallicity, see Sect. 2, above) is 0.36 dex higher than what found by Colucci et al. (2009), i.e. [Fe/H] = −1.85 ± 0.19 vs. [Fe/H] = −2.21 ± 0.03; however the difference is less than 2σ. It appears that our own scale and that based on high-resolution spectroscopy introduced by these authors are in *excellent* agreement. We note also that our metallicity estimate for the remote M 31 cluster MGC1, [Fe/H] = −2.16 ± 0.28 (Galleti et al. 2007), is in excellent agreement with what recently obtained by Mackey et al. (2009) from a high-quality CMD, [M/H] ≃ −2.3.

Appendix A: Homogeneous Lick indices in the T98 system for M 31 GCs

Table A.1. Lick indices for M 31 globular clusters from new observations (Sect. 3.1).

Cluster	Mg_2 mag	eMg_2 mag	Mg*b* Å	eMg*b* Å	Fe5270 Å	eFe5270 Å	Fe5335 Å	eFe5335 Å	Fe5406 Å	eFe5406 Å	Hβ Å	eHβ Å	y[1]	Set
B003	0.086	0.013	1.554	0.547	1.906	0.648	1.676	0.774	0.643	0.603	2.72	0.39	0	WHT
B006	0.210	0.005	3.051	0.221	2.112	0.262	1.942	0.305	1.389	0.230	1.83	0.17	0	WHT
B012	0.064	0.004	0.619	0.188	0.811	0.223	0.421	0.266	0.303	0.202	2.63	0.13	0	WHT
B017	0.159	0.007	1.979	0.291	1.798	0.338	1.862	0.393	0.957	0.300	1.73	0.22	0	WHT
B019	0.159	0.005	2.313	0.187	1.790	0.222	1.704	0.259	0.916	0.199	1.73	0.14	0	WHT
B020	0.120	0.002	1.962	0.082	1.929	0.092	1.710	0.105	1.406	0.078	1.98	0.07	0	TNG
B022	0.061	0.014	1.339	0.597	1.371	0.712	1.109	0.853	0.209	0.664	3.09	0.42	0	WHT
B023	0.137	0.004	1.929	0.171	1.824	0.186	1.432	0.211	1.205	0.154	1.96	0.17	0	LOI
B032	0.210	0.016	4.270	0.619	2.693	0.730	2.805	0.840	1.221	0.642	1.73	0.53	0	WHT
B034	0.201	0.013	3.339	0.533	2.450	0.631	1.916	0.744	1.656	0.555	1.15	0.41	0	WHT
B039	0.176	0.008	2.630	0.320	1.920	0.370	1.742	0.429	0.880	0.326	1.40	0.26	0	WHT
B042	0.161	0.008	2.204	0.325	1.629	0.374	1.458	0.432	0.997	0.323	1.87	0.27	0	WHT
B051	0.170	0.010	2.565	0.397	1.608	0.467	1.054	0.553	0.746	0.416	1.37	0.31	0	WHT
B058	0.097	0.007	1.452	0.294	1.220	0.352	1.478	0.402	0.812	0.312	2.34	0.24	0	LOI
B060	0.134	0.012	2.067	0.518	1.474	0.622	0.691	0.744	0.916	0.560	2.53	0.37	5	WHT
B070	0.123	0.010	1.358	0.406	0.976	0.481	0.944	0.564	0.292	0.436	2.53	0.29	5	WHT
B071	0.275	0.013	4.838	0.499	2.710	0.598	2.279	0.702	1.725	0.532	2.04	0.38	0	WHT
B073	0.207	0.012	3.623	0.465	2.767	0.546	2.572	0.635	1.235	0.490	2.21	0.35	0	WHT
B082	0.193	0.012	2.608	0.467	2.111	0.526	1.955	0.604	0.835	0.459	1.63	0.40	0	WHT
B083	0.037	0.011	0.787	0.442	0.977	0.494	0.677	0.575	0.826	0.423	1.72	0.42	2	WHT
B095	0.186	0.017	2.754	0.710	1.149	0.846	1.592	0.973	2.058	0.700	1.59	0.55	0	WHT
B099	0.166	0.010	2.216	0.412	1.680	0.485	1.374	0.571	0.824	0.437	1.74	0.30	0	WHT
B110	0.183	0.009	2.655	0.359	1.738	0.424	1.788	0.491	1.302	0.370	1.64	0.28	0	WHT
B111	0.144	0.019	2.342	0.774	1.845	0.923	1.084	1.079	0.804	0.819	1.60	0.60	0	WHT
B117	0.067	0.005	0.897	0.206	0.630	0.232	0.621	0.265	0.253	0.196	2.06	0.20	4	WHT
B131	0.279	0.005	4.067	0.204	2.389	0.243	2.118	0.285	1.485	0.218	1.57	0.15	0	WHT
B147	0.242	0.002	3.952	0.082	3.032	0.091	2.816	0.103	2.162	0.076	1.66	0.08	0	TNG
B148	0.240	0.008	4.036	0.299	2.946	0.326	2.743	0.368	0.911	0.283	3.74	0.28	0	WHT
B151	0.199	0.006	3.179	0.227	1.981	0.269	1.879	0.312	1.347	0.235	1.75	0.18	0	WHT
B153	0.247	0.011	4.057	0.432	2.427	0.513	2.228	0.598	1.860	0.450	1.55	0.34	0	WHT
B155	0.212	0.010	2.732	0.405	3.711	0.420	3.685	0.469	1.221	0.364	3.24	0.38	0	WHT
B156	0.078	0.009	1.259	0.376	1.400	0.410	1.224	0.465	0.571	0.345	1.99	0.38	0	WHT
B158	0.149	0.012	1.744	0.499	2.278	0.570	1.982	0.670	1.575	0.507	1.01	0.38	0	WHT
B162	0.270	0.015	4.720	0.602	2.198	0.738	2.727	0.843	1.623	0.646	1.91	0.46	0	WHT
B163	0.235	0.005	4.301	0.187	2.797	0.206	2.466	0.231	1.555	0.170	1.59	0.20	0	WHT
B169	0.280	0.013	5.389	0.486	2.657	0.543	1.977	0.624	2.404	0.447	1.65	0.52	0	WHT
B171	0.214	0.002	3.610	0.091	2.663	0.102	2.245	0.116	1.979	0.085	1.89	0.09	0	TNG
B174	0.103	0.006	1.950	0.243	1.417	0.270	1.194	0.306	0.892	0.225	1.89	0.25	0	WHT
B178	0.079	0.006	1.354	0.226	1.191	0.249	1.639	0.280	0.420	0.209	2.98	0.23	0	WHT
B179	0.116	0.008	1.933	0.317	1.408	0.350	1.520	0.396	0.648	0.299	1.10	0.32	0	WHT
B180	0.125	0.006	2.589	0.216	1.924	0.244	1.146	0.283	0.603	0.215	1.57	0.21	0	WHT
B182	0.146	0.014	2.776	0.554	1.593	0.667	0.878	0.799	0.328	0.607	1.92	0.42	0	WHT
B183	0.182	0.006	3.134	0.221	2.361	0.244	1.423	0.283	0.922	0.211	1.92	0.22	0	WHT
B185	0.159	0.007	2.834	0.289	2.258	0.316	1.745	0.358	0.893	0.261	1.70	0.31	0	WHT
B187	0.123	0.012	1.370	0.494	0.892	0.547	0.653	0.624	0.447	0.461	2.52	0.45	0	WHT
B193	0.233	0.004	4.182	0.167	3.071	0.183	2.631	0.207	1.558	0.155	1.92	0.17	0	WHT
B204	0.139	0.005	2.642	0.204	2.256	0.223	2.733	0.249	1.415	0.185	1.94	0.21	0	WHT
B206	0.082	0.004	1.494	0.143	1.516	0.157	1.293	0.179	0.837	0.131	2.23	0.14	0	WHT
B212	0.050	0.005	1.009	0.219	0.183	0.252	0.245	0.288	0.358	0.212	2.43	0.21	0	WHT
B215	0.196	0.007	3.493	0.288	2.306	0.320	1.758	0.364	0.861	0.273	1.92	0.29	0	WHT
B218	0.130	0.002	2.137	0.065	1.923	0.073	1.598	0.083	1.331	0.062	2.05	0.06	0	TNG
B219	0.157	0.009	3.211	0.339	2.070	0.386	1.241	0.449	1.057	0.344	2.41	0.32	0	WHT
B224	0.042	0.006	0.909	0.263	0.448	0.299	1.162	0.339	0.177	0.258	2.17	0.24	0	WHT
B225	0.170	0.002	3.279	0.077	2.464	0.085	2.167	0.098	1.021	0.074	1.77	0.08	0	WHT
B228	0.129	0.007	2.104	0.300	1.759	0.328	1.473	0.375	1.594	0.272	2.19	0.29	0	WHT
B230	0.057	0.007	0.107	0.286	0.461	0.315	0.174	0.363	0.267	0.268	2.53	0.26	0	WHT
B232	0.032	0.005	0.493	0.214	0.404	0.236	0.690	0.267	0.236	0.197	2.38	0.21	4	WHT
B233	0.099	0.005	1.709	0.192	1.883	0.210	1.629	0.240	0.825	0.181	2.04	0.18	0	WHT
B235	0.133	0.006	2.380	0.222	1.690	0.246	1.773	0.279	0.973	0.207	1.96	0.22	0	WHT
B236	0.052	0.012	0.767	0.486	0.318	0.534	0.009	0.613	0.320	0.441	4.40	0.46	0	WHT
B238	0.137	0.006	3.478	0.231	1.714	0.267	1.862	0.301	0.873	0.225	1.78	0.24	0	WHT

Table A.1. continued.

Cluster	Mg_2 mag	eMg_2 mag	Mg*b* Å	eMg*b* Å	Fe5270 Å	eFe5270 Å	Fe5335 Å	eFe5335 Å	Fe5406 Å	eFe5406 Å	Hβ Å	eHβ Å	y[1]	Set
B240	0.044	0.005	1.060	0.185	1.252	0.206	0.677	0.239	0.212	0.179	2.38	0.18	0	WHT
B318	0.027	0.004	0.112	0.165	0.586	0.190	0.231	0.222	0.601	0.165	5.49	0.12	1	TNG
B338	0.082	0.002	1.250	0.078	1.454	0.088	1.223	0.102	1.194	0.075	2.24	0.07	0	TNG
B344	0.109	0.007	1.669	0.270	2.161	0.291	2.320	0.330	1.114	0.249	1.85	0.26	0	WHT
B347	0.052	0.007	1.175	0.274	0.447	0.311	0.994	0.351	0.179	0.265	2.46	0.26	4	WHT
B348	0.136	0.008	2.169	0.303	2.221	0.327	1.443	0.383	1.061	0.284	2.52	0.28	0	WHT
B356	0.075	0.008	0.877	0.325	1.133	0.353	0.817	0.405	0.378	0.297	2.44	0.31	0	WHT
B358	0.023	0.003	0.230	0.122	0.599	0.137	0.296	0.159	0.649	0.116	2.91	0.11	0	TNG
B373	0.167	0.016	2.451	0.619	2.169	0.832	1.940	0.810	1.435	0.611	1.55	0.53	0	WHT
B381	0.075	0.006	1.372	0.257	1.766	0.283	1.650	0.323	0.722	0.242	1.67	0.25	0	WHT
B399	0.043	0.004	0.817	0.178	0.854	0.201	1.164	0.229	0.752	0.170	2.89	0.16	0	TNG
B457	0.265	0.000	4.029	0.013	3.851	0.014	3.496	0.016	2.891	0.012	1.44	0.01	0	TNG
B468	0.113	0.007	2.583	0.277	1.472	0.320	1.095	0.367	0.657	0.274	2.50	0.25	4	TNG
B472	0.080	0.004	3.214	0.142	1.378	0.168	1.266	0.192	0.514	0.143	2.23	0.15	0	WHT
G001	0.133	0.003	2.187	0.104	1.866	0.115	1.915	0.131	0.936	0.098	2.37	0.10	0	LOI
B020D	0.092	0.016	1.713	0.653	0.340	0.805	0.897	0.917	0.602	0.696	3.22	0.49	0	WHT
VDB0	0.031	0.002	0.186	0.088	0.598	0.101	0.568	0.116	0.366	0.087	4.50	0.07	1	TNG
B025D*	0.250	0.024	4.182	0.955	1.875	1.094	2.463	1.258	0.035	1.008	0.08	0.86	0	WHT
B041D	0.126	0.020	0.685	0.851	1.416	0.945	1.897	1.075	1.019	0.817	1.97	0.65	0	WHT
B046D*	0.230	0.026	3.245	1.091	2.712	1.255	3.013	1.454	1.154	1.160	2.12	0.76	0	WHT
B090D	0.291	0.007	4.122	0.298	2.604	0.349	2.241	0.408	1.732	0.310	1.51	0.23	0	WHT
B215D*	0.187	0.009	2.449	0.392	1.676	0.463	1.450	0.547	1.061	0.414	1.79	0.28	0	WHT
B344D	0.121	0.001	2.517	0.022	2.054	0.024	1.679	0.028	1.372	0.021	2.66	0.02	0	TNG
B514	0.062	0.003	0.300	0.137	0.176	0.154	1.279	0.169	0.282	0.159	2.32	0.13	0	LOI
MCGC1	0.041	0.007	0.566	0.290	0.489	0.327	0.005	0.379	0.397	0.276	1.84	0.29	0	LOI
MCGC8	0.093	0.003	1.334	0.115	1.400	0.128	1.206	0.147	1.041	0.109	1.98	0.10	0	TNG
MCGC10	0.031	0.003	0.395	0.104	0.633	0.118	0.427	0.136	0.677	0.100	2.93	0.09	0	TNG

[1] y = BLCC (young cluster) from Fusi Pecci et al. (2005) 0 – old cluster; 1 – color selected; 2 – H_β selected; 3 – color and H_β selected; 4 – reportedly young objects by other authors and candidates BLCC (Table 2).

* B025D, B046D and B215D are classified by Caldwell et al. (2009) as non-clusters and in the following analysis are not considered.

Table A.2. Lick indices M 31 globular clusters taken from literature sources and reported into the T98 system (Sect. 3.2).

Cluster	Mg_2 mag	eMg_2 mag	Mgb Å	eMgb Å	Fe5270 Å	eFe5270 Å	Fe5335 Å	eFe5335 Å	Fe5406 Å	eFe5406 Å	Hβ Å	eHβ Å	y[1]	Set[2]
B001	0.160	0.033	2.485	0.631	2.366	0.422	2.753	0.485	99.999	99.999	2.17	0.30	0	4
B003	0.086	0.013	1.554	0.547	1.906	0.648	1.676	0.774	0.643	0.603	2.75	0.39	0	3
B004	0.081	0.033	2.094	0.631	0.772	0.422	1.846	0.485	99.999	99.999	3.16	0.30	0	4
B005	0.153	0.033	2.379	0.631	2.033	0.422	1.021	0.485	99.999	99.999	2.05	0.30	0	4
B006	0.144	0.016	2.449	0.620	2.060	0.630	2.010	0.630	1.163	0.630	2.00	0.56	0	1
B008	0.144	0.033	2.005	0.631	2.893	0.422	2.984	0.485	99.999	99.999	3.67	0.30	2	4
B009	0.060	0.021	1.246	0.035	1.160	0.031	99.999	99.999	99.999	99.999	3.31	0.03	0	5
B010	0.073	0.033	0.628	0.631	1.561	0.422	1.021	0.485	99.999	99.999	3.00	0.30	0	4
B011	0.046	0.021	1.081	0.035	1.649	0.032	99.999	99.999	99.999	99.999	1.79	0.04	0	5
B012	0.064	0.004	0.619	0.188	0.811	0.223	0.421	0.266	0.303	0.202	2.66	0.13	0	3
B013	0.185	0.033	1.085	0.631	4.366	0.422	3.050	0.485	99.999	99.999	2.89	0.30	0	4
B015	0.362	0.010	6.430	0.292	4.160	0.275	3.300	0.317	1.990	0.237	1.53	0.27	4	0
B016	0.130	0.033	2.952	0.631	1.899	0.422	1.778	0.485	99.999	99.999	1.72	0.30	0	4
B017	0.159	0.007	1.979	0.291	1.798	0.338	1.862	0.393	0.957	0.300	1.76	0.22	0	3
B018	0.090	0.033	1.733	0.631	1.999	0.422	2.453	0.485	99.999	99.999	2.40	0.30	7	4
B019	0.159	0.005	2.313	0.187	1.790	0.222	1.704	0.259	0.916	0.199	1.76	0.14	0	3
B020	0.120	0.002	1.962	0.082	1.929	0.092	1.710	0.105	1.406	0.078	1.98	0.07	0	6
B021	0.109	0.033	2.659	0.631	1.254	0.422	1.778	0.485	99.999	99.999	1.91	0.30	0	4
B022	0.061	0.014	1.339	0.597	1.371	0.712	1.109	0.853	0.209	0.664	3.12	0.42	0	3
B023	0.137	0.004	1.929	0.171	1.824	0.186	1.432	0.211	1.205	0.154	1.96	0.17	0	7
B024	0.163	0.019	2.741	0.032	1.997	0.028	99.999	99.999	99.999	99.999	1.22	0.03	0	5
B025	0.088	0.019	0.997	0.870	1.480	0.880	0.610	0.880	0.253	0.880	3.24	0.78	0	1
B026	0.213	0.033	4.461	0.631	1.832	0.422	2.620	0.485	99.999	99.999	1.48	0.30	0	4
B027	0.052	0.014	0.860	0.022	0.776	0.020	99.999	99.999	99.999	99.999	2.39	0.02	0	5
B028	0.092	0.033	1.347	0.631	1.764	0.422	–0.395	0.485	99.999	99.999	3.98	0.30	2	4
B029	0.171	0.033	3.607	0.631	3.988	0.422	2.486	0.485	99.999	99.999	0.50	0.30	0	4
B030	0.228	0.033	2.694	0.631	3.797	0.422	3.083	0.485	99.999	99.999	1.79	0.30	4	4
B031	0.111	0.033	2.572	0.631	–0.346	0.422	0.847	0.485	99.999	99.999	0.80	0.30	0	4
B032	0.210	0.016	4.270	0.619	2.693	0.730	2.805	0.840	1.221	0.642	1.76	0.53	0	3
B033	0.079	0.033	1.217	0.631	1.798	0.422	1.948	0.485	99.999	99.999	3.30	0.30	0	4
B034	0.122	0.011	1.830	0.490	1.490	0.500	1.680	0.500	0.863	0.500	2.18	0.47	0	1
B035	0.080	0.033	1.825	0.631	1.254	0.422	3.669	0.485	99.999	99.999	2.45	0.30	0	4
B037	0.100	0.033	1.825	0.631	3.477	0.422	1.914	0.485	99.999	99.999	99.99	9.99	0	4
B038	0.090	0.033	0.782	0.631	1.289	0.422	–0.143	0.485	99.999	99.999	2.89	0.30	0	4
B039	0.176	0.008	2.630	0.320	1.920	0.370	1.742	0.429	0.880	0.326	1.43	0.26	0	3
B040	0.019	0.033	0.743	0.631	–0.321	0.422	1.982	0.485	99.999	99.999	7.58	0.30	3	4
B041	0.047	0.033	1.217	0.631	1.595	0.422	1.982	0.485	99.999	99.999	2.73	0.30	0	4
B042	0.161	0.008	2.204	0.325	1.629	0.374	1.458	0.432	0.997	0.323	1.90	0.27	0	3
B043	0.040	0.033	0.512	0.631	0.807	0.422	0.567	0.485	99.999	99.999	5.70	0.30	3	4
B044	0.105	0.031	4.037	0.049	2.148	0.046	99.999	99.999	99.999	99.999	99.99	9.99	0	5
B045	0.138	0.014	1.417	0.640	2.290	0.640	1.530	0.640	1.323	0.650	2.34	0.56	0	1
B046	0.115	0.039	–0.126	0.065	1.071	0.061	99.999	99.999	99.999	99.999	1.98	0.06	0	5
B047	0.207	0.036	2.427	0.061	–2.290	0.056	99.999	99.999	99.999	99.999	2.69	0.06	2	5
B048	0.151	0.019	2.219	0.860	2.370	0.860	2.380	0.880	0.493	0.880	2.90	0.77	0	1
B049	0.052	0.033	1.272	0.631	1.629	0.422	–0.793	0.485	99.999	99.999	9.48	0.30	3	4
B050	0.089	0.033	1.951	0.631	0.144	0.422	1.846	0.485	99.999	99.999	1.86	0.30	0	4
B051	0.170	0.016	1.983	0.730	2.530	0.740	1.630	0.740	1.393	0.740	1.80	0.67	0	1
B054	0.207	0.033	3.391	0.631	3.024	0.422	2.786	0.485	99.999	99.999	1.77	0.30	0	4
B055	0.161	0.033	3.408	0.631	1.561	0.422	2.719	0.485	99.999	99.999	2.80	0.30	0	4
B056	0.229	0.033	3.755	0.631	3.829	0.422	2.819	0.485	99.999	99.999	1.77	0.30	0	4
B057	0.076	0.033	1.291	0.631	2.795	0.422	–0.539	0.485	99.999	99.999	5.73	0.30	2	4
B058	0.070	0.009	1.860	0.270	1.900	0.254	0.980	0.275	0.910	0.220	2.16	0.25	0	0
B059	0.144	0.033	3.391	0.631	1.865	0.422	0.496	0.485	99.999	99.999	1.21	0.30	0	4
B060	0.134	0.012	2.067	0.518	1.474	0.622	0.691	0.744	0.916	0.560	2.56	0.37	1	3
B061	0.187	0.033	2.728	0.631	2.598	0.422	1.436	0.485	99.999	99.999	3.12	0.30	0	4
B063	0.141	0.020	1.735	0.032	1.317	0.029	99.999	99.999	99.999	99.999	1.20	0.03	0	5
B064	0.077	0.020	0.357	0.033	1.802	0.030	99.999	99.999	99.999	99.999	1.77	0.03	0	5
B065	0.080	0.033	1.402	0.631	1.663	0.422	0.952	0.485	99.999	99.999	2.22	0.30	0	4
B066	0.055	0.033	0.991	0.631	0.319	0.422	–0.467	0.485	99.999	99.999	4.84	0.30	3	4
B068	0.187	0.024	4.062	0.041	1.428	0.034	99.999	99.999	99.999	99.999	0.49	0.04	0	5
B069	0.135	0.033	1.384	0.631	1.730	0.422	2.386	0.485	99.999	99.999	7.34	0.30	3	4
B070	0.123	0.010	1.358	0.406	0.976	0.481	0.944	0.564	0.292	0.436	2.56	0.29	1	3
B071	0.275	0.013	4.838	0.499	2.710	0.598	2.279	0.702	1.725	0.532	2.06	0.38	0	3
B072	0.164	0.033	2.641	0.631	3.284	0.422	2.520	0.485	99.999	99.999	2.15	0.30	0	4

Table A.2. continued.

Cluster	Mg_2 mag	eMg_2 mag	Mgb Å	eMgb Å	Fe5270 Å	eFe5270 Å	Fe5335 Å	eFe5335 Å	Fe5406 Å	eFe5406 Å	Hβ Å	eHβ Å	y[1]	Set[2]
B073	0.207	0.012	3.623	0.465	2.767	0.546	2.572	0.635	1.235	0.490	2.24	0.35	0	3
B074	0.078	0.033	0.609	0.631	1.152	0.422	0.426	0.485	99.999	99.999	4.09	0.30	2	4
B075	0.048	0.033	1.697	0.631	–0.784	0.422	2.620	0.485	99.999	99.999	2.17	0.30	0	4
B076	0.133	0.033	2.641	0.631	0.249	0.422	2.218	0.485	99.999	99.999	3.21	0.30	0	4
B081	0.036	0.033	0.648	0.631	0.945	0.422	1.778	0.485	99.999	99.999	8.15	0.30	3	4
B082	0.193	0.012	2.608	0.467	2.111	0.526	1.955	0.604	0.835	0.459	1.66	0.40	0	3
B083	0.037	0.011	0.787	0.442	0.977	0.494	0.677	0.575	0.826	0.423	1.75	0.42	2	3
B085	0.014	0.021	0.916	0.034	1.160	0.031	99.999	99.999	99.999	99.999	3.31	0.03	0	5
B086	0.038	0.015	–0.443	0.025	1.183	0.022	99.999	99.999	99.999	99.999	2.55	0.03	0	5
B088	0.043	0.033	0.820	0.631	0.108	0.422	0.742	0.485	99.999	99.999	2.77	0.30	0	4
B090	0.218	0.033	3.308	0.631	3.381	0.422	1.982	0.485	99.999	99.999	3.45	0.30	4	4
B091	0.116	0.033	1.384	0.631	1.932	0.422	1.880	0.485	99.999	99.999	7.47	0.30	3	4
B092	0.100	0.024	1.843	0.039	0.410	0.035	99.999	99.999	99.999	99.999	1.79	0.04	0	5
B093	0.123	0.033	1.933	0.631	2.167	0.422	2.016	0.485	99.999	99.999	3.14	0.30	0	4
B094	0.131	0.033	2.797	0.631	2.598	0.422	2.386	0.485	99.999	99.999	2.31	0.30	0	4
B095	0.186	0.017	2.754	0.710	1.149	0.846	1.592	0.973	2.058	0.700	1.62	0.55	0	3
B096	0.215	0.031	2.974	0.055	3.055	0.042	99.999	99.999	99.999	99.999	1.44	0.05	0	5
B097	0.124	0.033	1.569	0.631	2.400	0.422	1.402	0.485	99.999	99.999	2.87	0.30	0	4
B098	0.182	0.027	4.602	0.045	1.649	0.040	99.999	99.999	99.999	99.999	1.53	0.04	0	5
B099	0.166	0.010	2.216	0.412	1.680	0.485	1.374	0.571	0.824	0.437	1.77	0.30	0	3
B103	0.184	0.013	3.333	0.021	1.250	0.018	99.999	99.999	99.999	99.999	1.56	0.02	0	5
B105	0.120	0.033	1.513	0.631	2.033	0.422	2.016	0.485	99.999	99.999	1.67	0.30	0	4
B106	0.135	0.033	0.943	0.056	1.932	0.050	99.999	99.999	99.999	99.999	0.67	0.05	0	5
B107	0.093	0.014	1.219	0.023	1.824	0.020	99.999	99.999	99.999	99.999	2.02	0.02	0	5
B109	0.250	0.033	2.711	0.631	2.828	0.422	2.719	0.485	99.999	99.999	99.99	9.99	0	4
B110	0.183	0.009	2.655	0.359	1.738	0.424	1.788	0.491	1.302	0.370	1.67	0.28	0	3
B111	0.144	0.019	2.342	0.774	1.845	0.923	1.084	1.079	0.804	0.819	1.63	0.60	0	3
B112	0.291	0.038	5.997	0.063	3.727	0.054	99.999	99.999	99.999	99.999	2.09	0.06	0	5
B115	0.273	0.013	3.862	0.022	1.976	0.018	99.999	99.999	99.999	99.999	0.12	0.02	0	5
B116	0.171	0.033	2.326	0.631	2.598	0.422	2.252	0.485	99.999	99.999	2.73	0.30	0	4
B117	0.067	0.005	0.897	0.206	0.630	0.232	0.621	0.265	0.253	0.196	2.09	0.20	4	3
B119	0.226	0.033	3.524	0.631	2.532	0.422	1.982	0.485	99.999	99.999	1.65	0.30	0	4
B122	0.171	0.033	1.679	0.631	2.100	0.422	0.249	0.485	99.999	99.999	2.61	0.30	0	4
B125	0.063	0.033	1.440	0.631	–0.367	0.422	0.777	0.485	99.999	99.999	3.21	0.30	0	4
B126	0.046	0.014	1.280	0.240	1.020	0.170	0.810	0.200	0.470	0.140	3.65	0.14	0	2
B127	0.189	0.004	2.716	0.210	3.020	0.210	0.950	0.210	1.203	0.210	1.68	0.20	0	1
B129	0.183	0.033	2.449	0.631	3.024	0.422	0.532	0.485	99.999	99.999	2.73	0.30	0	4
B130	0.070	0.033	1.458	0.631	0.876	0.422	1.880	0.485	99.999	99.999	3.43	0.30	0	4
B131	0.279	0.005	4.067	0.204	2.389	0.243	2.118	0.285	1.485	0.218	1.60	0.15	0	3
B134	0.109	0.014	2.220	0.240	1.790	0.170	1.590	0.200	0.990	0.150	1.78	0.16	0	2
B135	0.076	0.033	1.160	0.631	1.323	0.422	0.777	0.485	99.999	99.999	2.26	0.30	0	4
B137	0.099	0.033	0.915	0.631	1.999	0.422	1.914	0.485	99.999	99.999	2.84	0.30	0	4
B140	0.247	0.033	3.706	0.631	3.251	0.422	0.812	0.485	99.999	99.999	0.18	0.30	0	4
B141	0.072	0.033	0.686	0.631	0.529	0.422	1.470	0.485	99.999	99.999	2.93	0.30	0	4
B143	0.241	0.015	4.136	0.026	2.256	0.023	99.999	99.999	99.999	99.999	1.53	0.03	0	5
B144	0.187	0.011	2.647	0.470	2.430	0.470	1.570	0.480	1.143	0.480	1.76	0.46	0	1
B146	0.171	0.042	5.672	0.066	3.985	0.059	99.999	99.999	99.999	99.999	0.20	0.07	4	5
B147	0.242	0.002	3.952	0.082	3.032	0.091	2.816	0.103	2.162	0.076	1.66	0.08	0	6
B148	0.145	0.010	2.151	0.390	1.960	0.390	2.040	0.390	1.263	0.390	2.01	0.37	0	1
B149	0.090	0.033	1.328	0.631	2.200	0.422	1.948	0.485	99.999	99.999	2.93	0.30	0	4
B151	0.199	0.006	3.179	0.227	1.981	0.269	1.879	0.312	1.347	0.235	1.78	0.18	0	3
B152	0.062	0.026	2.295	0.042	2.170	0.039	99.999	99.999	99.999	99.999	1.22	0.04	0	5
B153	0.247	0.011	4.057	0.432	2.427	0.513	2.228	0.598	1.860	0.450	1.58	0.34	0	3
B154	0.265	0.029	4.963	0.047	3.034	0.044	99.999	99.999	99.999	99.999	1.65	0.05	4	5
B155	0.212	0.010	2.732	0.405	3.711	0.420	3.685	0.469	1.221	0.364	3.27	0.38	0	3
B156	0.078	0.009	1.259	0.376	1.400	0.410	1.224	0.465	0.571	0.345	2.02	0.38	0	3
B158	0.130	0.013	2.270	0.210	1.860	0.100	1.700	0.130	1.060	0.090	1.74	0.10	0	2
B159	0.177	0.033	2.113	0.631	2.300	0.422	1.367	0.485	99.999	99.999	2.57	0.30	0	4
B161	0.180	0.033	2.237	0.631	2.167	0.422	1.436	0.485	99.999	99.999	1.98	0.30	0	4
B162	0.270	0.015	4.720	0.602	2.198	0.738	2.727	0.843	1.623	0.646	1.94	0.46	0	3
B163	0.222	0.013	4.010	0.190	2.600	0.070	2.440	0.090	1.570	0.060	1.74	0.07	0	2
B164	0.216	0.033	3.308	0.631	1.561	0.422	2.319	0.485	99.999	99.999	1.65	0.30	4	4
B165	0.050	0.025	–0.328	0.041	1.693	0.038	99.999	99.999	99.999	99.999	2.51	0.04	0	5
B167	0.180	0.033	3.037	0.631	3.154	0.422	2.083	0.485	99.999	99.999	2.03	0.30	0	4
B169	0.280	0.013	5.389	0.486	2.657	0.543	1.977	0.624	2.404	0.447	1.68	0.52	0	3

Table A.2. continued.

Cluster	Mg_2 mag	eMg_2 mag	Mgb Å	eMgb Å	Fe5270 Å	eFe5270 Å	Fe5335 Å	eFe5335 Å	Fe5406 Å	eFe5406 Å	Hβ Å	eHβ Å	y[1]	Set[2]
B170	0.116	0.033	3.424	0.631	0.354	0.422	2.050	0.485	99.999	99.999	4.69	0.30	2	4
B171	0.189	0.011	3.110	0.314	2.340	0.296	2.400	0.338	1.550	0.256	2.27	0.29	0	0
B171	0.214	0.002	3.610	0.091	2.663	0.102	2.245	0.116	1.979	0.085	1.89	0.09	0	6
B174	0.103	0.006	1.950	0.243	1.417	0.270	1.194	0.306	0.892	0.225	1.92	0.25	0	3
B178	0.097	0.009	1.890	0.270	1.930	0.254	0.310	0.229	0.730	0.220	1.97	0.25	0	0
B179	0.116	0.008	1.933	0.317	1.408	0.350	1.520	0.396	0.648	0.299	1.13	0.32	0	3
B180	0.125	0.006	2.589	0.216	1.924	0.244	1.146	0.283	0.603	0.215	1.60	0.21	0	3
B182	0.076	0.011	1.700	0.460	1.740	0.470	1.660	0.470	0.803	0.470	2.39	0.42	0	1
B183	0.182	0.006	3.134	0.221	2.361	0.244	1.423	0.283	0.922	0.211	1.95	0.22	0	3
B184	0.219	0.033	4.398	0.631	2.532	0.422	2.553	0.485	99.999	99.999	1.79	0.30	0	4
B185	0.159	0.007	2.834	0.289	2.258	0.316	1.745	0.358	0.893	0.261	1.73	0.31	0	3
B187	0.123	0.012	1.370	0.494	0.892	0.547	0.653	0.624	0.447	0.461	2.55	0.45	0	3
B188	0.094	0.033	1.624	0.631	0.038	0.422	1.298	0.485	99.999	99.999	2.43	0.30	0	4
B190	0.094	0.033	1.915	0.631	2.066	0.422	1.812	0.485	99.999	99.999	2.52	0.30	0	4
B193	0.233	0.004	4.182	0.167	3.071	0.183	2.631	0.207	1.558	0.155	1.95	0.17	0	3
B197	0.234	0.033	3.998	0.631	2.991	0.422	2.786	0.485	99.999	99.999	1.31	0.30	4	4
B198	0.160	0.033	2.255	0.631	2.532	0.422	2.184	0.485	99.999	99.999	2.33	0.30	0	4
B199	0.068	0.033	0.877	0.631	0.494	0.422	1.091	0.485	99.999	99.999	3.16	0.30	0	4
B200	0.111	0.033	2.728	0.631	1.391	0.422	3.181	0.485	99.999	99.999	2.17	0.30	0	4
B201	0.106	0.017	2.216	0.028	2.019	0.027	99.999	99.999	99.999	99.999	1.88	0.03	0	5
B203	0.175	0.033	2.745	0.631	2.400	0.422	0.987	0.485	99.999	99.999	1.04	0.30	0	4
B204	0.139	0.005	2.642	0.204	2.256	0.223	2.733	0.249	1.415	0.185	1.97	0.21	0	3
B205	0.097	0.008	1.789	0.013	1.272	0.012	99.999	99.999	99.999	99.999	1.58	0.01	0	5
B206	0.082	0.004	1.494	0.143	1.516	0.157	1.293	0.179	0.837	0.131	2.26	0.14	0	3
B207	0.078	0.033	1.422	0.631	1.932	0.422	1.333	0.485	99.999	99.999	3.23	0.30	0	4
B208	0.220	0.033	2.606	0.631	3.638	0.422	1.914	0.485	99.999	99.999	3.21	0.30	0	4
B209	0.090	0.033	2.077	0.631	1.561	0.422	1.160	0.485	99.999	99.999	2.03	0.30	0	4
B210	0.052	0.033	0.782	0.631	1.186	0.422	1.229	0.485	99.999	99.999	7.00	0.30	3	4
B211	0.028	0.024	1.546	0.039	2.617	0.037	99.999	99.999	99.999	99.999	3.05	0.03	0	5
B212	0.050	0.005	1.009	0.219	0.183	0.252	0.245	0.288	0.358	0.212	2.46	0.21	0	3
B213	0.159	0.033	2.397	0.631	2.233	0.422	1.402	0.485	99.999	99.999	1.26	0.30	0	4
B214	0.071	0.033	1.217	0.631	1.932	0.422	2.586	0.485	99.999	99.999	3.41	0.30	4	4
B215	0.196	0.007	3.493	0.288	2.306	0.320	1.758	0.364	0.861	0.273	1.95	0.29	0	3
B217	0.095	0.033	2.184	0.631	1.595	0.422	1.607	0.485	99.999	99.999	1.98	0.30	0	4
B218	0.123	0.009	2.300	0.261	1.990	0.245	1.710	0.276	1.460	0.213	1.86	0.24	0	0
B219	0.157	0.009	3.211	0.339	2.070	0.386	1.241	0.449	1.057	0.344	2.44	0.32	0	3
B220	0.092	0.033	1.752	0.631	1.391	0.422	1.333	0.485	99.999	99.999	2.26	0.30	0	4
B221	0.135	0.033	1.897	0.631	2.532	0.422	1.229	0.485	99.999	99.999	2.08	0.30	0	4
B222	0.101	0.015	1.300	0.390	1.870	0.370	1.170	0.430	0.970	0.310	4.46	0.31	2	2
B224	0.042	0.006	0.909	0.263	0.448	0.299	1.162	0.339	0.177	0.258	2.20	0.24	0	3
B225	0.187	0.013	3.210	0.190	2.310	0.070	2.030	0.090	1.310	0.060	1.83	0.07	0	2
B228	0.129	0.007	2.104	0.300	1.759	0.328	1.473	0.375	1.594	0.272	2.21	0.29	0	3
B230	0.057	0.007	0.107	0.286	0.461	0.315	0.174	0.363	0.267	0.268	2.56	0.26	0	3
B231	0.102	0.033	2.077	0.631	1.629	0.422	1.710	0.485	99.999	99.999	2.59	0.30	0	4
B232	0.032	0.005	0.493	0.214	0.404	0.236	0.690	0.267	0.236	0.197	2.41	0.21	4	3
B233	0.061	0.015	0.554	0.025	1.736	0.022	99.999	99.999	99.999	99.999	2.16	0.03	0	5
B234	0.113	0.014	2.370	0.240	2.030	0.180	1.500	0.210	0.990	0.150	1.72	0.16	0	2
B235	0.133	0.006	2.380	0.222	1.690	0.246	1.773	0.279	0.973	0.207	1.99	0.22	0	3
B236	0.052	0.012	0.767	0.486	0.318	0.534	0.009	0.613	0.320	0.441	4.43	0.46	0	3
B237	0.070	0.033	–0.357	0.631	3.251	0.422	0.952	0.485	99.999	99.999	7.60	0.30	2	4
B238	0.137	0.006	3.478	0.231	1.714	0.267	1.862	0.301	0.873	0.225	1.81	0.24	0	3
B239	0.068	0.026	1.219	0.043	1.183	0.038	99.999	99.999	99.999	99.999	1.67	0.04	0	5
B240	0.051	0.007	0.750	0.204	0.742	0.190	0.954	0.208	0.723	0.168	2.05	0.19	0	0
B272	0.154	0.033	2.130	0.631	2.300	0.422	1.160	0.485	99.999	99.999	2.05	0.30	0	4
B281	0.160	0.033	1.951	0.631	3.956	0.422	0.952	0.485	99.999	99.999	5.73	0.30	2	4
B283	0.191	0.033	3.475	0.631	–0.140	0.422	3.312	0.485	99.999	99.999	99.99	9.99	0	4
B292	0.053	0.016	0.970	0.400	0.950	0.390	1.140	0.450	0.150	0.340	3.14	0.32	4	2
B293	0.057	0.021	0.860	0.033	1.093	0.032	99.999	99.999	99.999	99.999	3.55	0.03	0	5
B295	0.029	0.033	1.328	0.631	0.633	0.422	0.496	0.485	99.999	99.999	4.94	0.30	2	4
B298	0.040	0.019	–0.356	0.031	0.981	0.026	99.999	99.999	99.999	99.999	2.30	0.03	0	5
B301	0.056	0.015	1.700	0.380	1.430	0.370	1.180	0.420	0.330	0.310	2.94	0.33	0	2
B303	0.119	0.033	1.733	0.631	1.561	0.422	–0.071	0.485	99.999	99.999	5.95	0.30	3	4
B304	0.050	0.015	1.230	0.370	1.400	0.360	0.920	0.420	0.850	0.300	2.52	0.30	0	2
B305	0.052	0.033	2.005	0.631	–0.892	0.422	3.475	0.485	99.999	99.999	2.77	0.30	0	4

Table A.2. continued.

Cluster	Mg_2 mag	eMg_2 mag	Mgb Å	eMgb Å	Fe5270 Å	eFe5270 Å	Fe5335 Å	eFe5335 Å	Fe5406 Å	eFe5406 Å	Hβ Å	eHβ Å	y[1]	Set[2]
B306	0.125	0.033	1.587	0.631	2.200	0.422	0.742	0.485	99.999	99.999	2.47	0.30	0	4
B307	0.053	0.033	2.659	0.631	1.798	0.422	3.050	0.485	99.999	99.999	5.93	0.30	2	4
B310	0.035	0.015	0.920	0.360	1.260	0.350	0.840	0.400	0.440	0.290	2.56	0.30	0	2
B311	0.049	0.012	0.798	0.560	1.100	0.560	0.610	0.560	0.403	0.560	2.80	0.52	4	1
B312	0.118	0.010	1.448	0.450	2.150	0.450	0.690	0.450	0.443	0.450	2.94	0.43	0	1
B313	0.120	0.014	2.170	0.280	1.690	0.230	1.450	0.260	0.970	0.190	1.51	0.21	0	2
B315	0.089	0.011	0.676	0.470	1.930	0.480	0.110	0.500	0.993	0.510	4.75	0.40	3	1
B316	0.151	0.033	2.237	0.631	2.433	0.422	0.917	0.485	99.999	99.999	2.64	0.30	7	4
B317	0.028	0.030	–0.241	0.048	1.539	0.046	99.999	99.999	99.999	99.999	1.67	0.05	0	5
B318	0.027	0.004	0.112	0.165	0.586	0.190	0.231	0.222	0.601	0.165	5.49	0.12	1	6
B319	0.066	0.033	0.877	0.631	0.668	0.422	0.602	0.485	99.999	99.999	5.54	0.30	2	4
B321	0.032	0.016	0.940	0.430	0.800	0.450	0.730	0.520	0.200	0.380	6.85	0.32	3	2
B322	0.028	0.015	0.350	0.340	0.630	0.330	0.670	0.380	0.450	0.280	5.06	0.24	1	2
B324	0.065	0.014	1.570	0.240	1.660	0.190	1.460	0.220	0.710	0.160	4.69	0.14	4	2
B327	0.057	0.014	0.590	0.250	0.830	0.190	1.100	0.220	0.720	0.160	3.78	0.14	3	2
B328	0.048	0.016	0.190	0.420	0.890	0.410	0.490	0.480	0.400	0.350	2.58	0.35	4	2
B335	0.140	0.033	2.624	0.631	1.186	0.422	1.298	0.485	99.999	99.999	2.31	0.30	0	4
B337	0.064	0.013	1.860	0.190	1.480	0.070	1.110	0.090	0.640	0.060	3.23	0.07	0	2
B338	0.085	0.009	1.220	0.260	1.640	0.245	1.450	0.273	0.730	0.213	2.10	0.24	0	0
B341	0.123	0.033	2.041	0.631	1.254	0.422	1.607	0.485	99.999	99.999	2.05	0.30	0	4
B343	0.086	0.015	1.573	0.024	1.824	0.022	99.999	99.999	99.999	99.999	1.48	0.02	0	5
B344	0.109	0.007	1.669	0.270	2.161	0.291	2.320	0.330	1.114	0.249	1.88	0.26	0	3
B347	0.024	0.014	0.760	0.260	0.510	0.210	0.490	0.240	0.370	0.170	2.87	0.17	4	2
B348	0.136	0.008	2.169	0.303	2.221	0.327	1.443	0.383	1.061	0.284	2.55	0.28	0	3
B350	0.055	0.015	1.130	0.340	0.980	0.320	0.810	0.370	0.330	0.270	2.80	0.27	0	2
B352	0.119	0.026	2.558	0.044	0.201	0.039	99.999	99.999	99.999	99.999	2.82	0.04	0	5
B356	0.075	0.008	0.877	0.325	1.133	0.353	0.817	0.405	0.378	0.297	2.47	0.31	0	3
B357	0.127	0.022	1.191	0.036	1.780	0.033	99.999	99.999	99.999	99.999	2.12	0.03	0	5
B358	0.034	0.007	0.767	0.207	0.810	0.194	0.397	0.187	0.291	0.171	2.63	0.20	1	0
B365	0.060	0.014	1.370	0.260	1.330	0.200	1.000	0.240	0.500	0.180	2.72	0.17	0	2
B366	0.015	0.033	0.763	0.631	–0.339	0.422	0.742	0.485	99.999	99.999	3.07	0.30	0	4
B367	0.050	0.033	0.260	0.631	2.466	0.422	1.021	0.485	99.999	99.999	6.38	0.30	3	4
B370	0.050	0.015	0.913	0.730	–0.080	0.730	0.730	0.740	0.543	0.740	2.71	0.71	0	1
B372	0.117	0.016	1.379	0.660	1.930	0.670	1.610	0.670	0.723	0.670	2.36	0.63	0	1
B373	0.167	0.016	2.451	0.619	2.169	0.832	1.940	0.810	1.435	0.611	1.58	0.53	0	3
B374	0.094	0.033	1.402	0.631	1.932	0.422	1.744	0.485	99.999	99.999	4.24	0.30	3	4
B375	0.128	0.025	0.888	0.044	1.539	0.037	99.999	99.999	99.999	99.999	2.35	0.04	0	5
B376	0.074	0.038	2.348	0.062	0.799	0.060	99.999	99.999	99.999	99.999	6.40	0.06	1	5
B377	0.060	0.030	–1.503	0.051	1.160	0.047	99.999	99.999	99.999	99.999	2.07	0.05	0	5
B378	0.068	0.033	0.972	0.631	1.357	0.422	1.539	0.485	99.999	99.999	3.09	0.30	0	4
B379	0.171	0.020	1.654	0.033	1.516	0.026	99.999	99.999	99.999	99.999	1.48	0.03	0	5
B381	0.075	0.006	1.372	0.257	1.766	0.283	1.650	0.323	0.722	0.242	1.70	0.25	0	3
B382	0.046	0.033	1.532	0.631	1.152	0.422	1.607	0.485	99.999	99.999	3.09	0.30	0	4
B383	0.163	0.013	3.030	0.220	2.120	0.140	1.790	0.170	1.210	0.120	1.75	0.13	0	2
B384	0.163	0.014	1.681	0.024	2.084	0.020	99.999	99.999	99.999	99.999	1.20	0.02	0	5
B386	0.105	0.013	1.410	0.021	2.019	0.019	99.999	99.999	99.999	99.999	2.07	0.02	0	5
B387	0.077	0.020	0.749	0.033	0.686	0.030	99.999	99.999	99.999	99.999	3.44	0.03	0	5
B391	0.077	0.033	1.179	0.631	1.323	0.422	3.637	0.485	99.999	99.999	2.75	0.30	0	4
B393	0.102	0.014	1.490	0.320	1.930	0.280	1.580	0.330	0.700	0.240	1.90	0.24	0	2
B397	0.125	0.025	1.519	0.042	0.868	0.037	99.999	99.999	99.999	99.999	2.30	0.04	0	5
B398	0.162	0.014	3.170	0.300	2.310	0.270	1.710	0.310	1.070	0.230	1.60	0.24	0	2
B399	0.043	0.004	0.817	0.178	0.854	0.201	1.164	0.229	0.752	0.170	2.89	0.16	0	6
B400	0.103	0.033	1.197	0.631	3.348	0.422	–0.215	0.485	99.999	99.999	0.65	0.30	0	4
B401	0.027	0.014	0.530	0.270	0.630	0.230	0.530	0.270	–0.030	0.200	2.84	0.19	0	2
B403	0.208	0.057	3.637	0.097	3.985	0.073	99.999	99.999	99.999	99.999	99.99	9.99	0	5
B405	0.086	0.009	1.274	0.015	0.663	0.021	99.999	99.999	99.999	99.999	2.14	0.01	0	5
B407	0.155	0.017	2.427	0.028	1.317	0.025	99.999	99.999	99.999	99.999	0.59	0.03	0	5
B431	0.066	0.030	–1.234	0.052	1.714	0.044	99.999	99.999	99.999	99.999	1.74	0.04	1	5
B448	0.087	0.033	0.915	0.631	1.083	0.422	–0.503	0.485	99.999	99.999	6.87	0.30	2	4
B457	0.265	0.000	4.029	0.013	3.851	0.014	3.496	0.016	2.891	0.012	1.44	0.01	0	6
B458	0.102	0.033	0.820	0.631	2.333	0.422	2.419	0.485	99.999	99.999	6.36	0.30	3	4
B467	0.074	0.033	0.338	0.631	–0.033	0.422	0.391	0.485	99.999	99.999	2.33	0.30	0	4
B468	0.113	0.007	2.583	0.277	1.472	0.320	1.095	0.367	0.657	0.274	2.50	0.25	4	6
B472	0.080	0.004	3.214	0.142	1.378	0.168	1.266	0.192	0.514	0.143	2.26	0.15	0	3

Table A.2. continued.

Cluster	Mg_2 mag	eMg_2 mag	Mg*b* Å	eMg*b* Å	Fe5270 Å	eFe5270 Å	Fe5335 Å	eFe5335 Å	Fe5406 Å	eFe5406 Å	Hβ Å	eHβ Å	y[1]	Set[2]
B475	0.109	0.033	0.279	0.631	1.083	0.422	0.496	0.485	99.999	99.999	6.13	0.30	3	4
B480	0.035	0.033	1.123	0.631	1.697	0.422	1.982	0.485	99.999	99.999	5.36	0.30	2	4
B483	0.089	0.033	0.004	0.631	1.014	0.422	–1.270	0.485	99.999	99.999	5.75	0.30	3	4
B484	0.044	0.033	1.235	0.631	0.980	0.422	1.539	0.485	99.999	99.999	5.87	0.30	3	4
B486	0.029	0.038	–1.473	0.064	–0.057	0.057	99.999	99.999	99.999	99.999	3.22	0.06	1	5
G001	0.133	0.003	2.187	0.104	1.866	0.115	1.915	0.131	0.936	0.098	2.37	0.10	0	7
G002	0.053	0.016	–0.155	0.026	1.138	0.023	99.999	99.999	99.999	99.999	2.12	0.03	0	5
B189D	0.079	0.033	1.217	0.631	0.807	0.422	2.252	0.485	99.999	99.999	4.41	0.30	1	4
B020D	0.092	0.016	1.713	0.653	0.340	0.805	0.897	0.917	0.602	0.696	3.25	0.49	0	3
B103D	0.193	0.033	3.291	0.631	2.631	0.422	2.386	0.485	99.999	99.999	1.74	0.30	0	4
G327	0.053	0.033	0.934	0.631	0.876	0.422	0.320	0.485	99.999	99.999	3.00	0.30	0	4
VDB0	0.031	0.002	0.186	0.088	0.598	0.101	0.568	0.116	0.366	0.087	4.50	0.07	1	6
NB16	0.066	0.013	1.610	0.200	1.180	0.090	0.970	0.110	0.500	0.080	3.34	0.08	4	2
NB89	0.123	0.013	2.430	0.200	1.910	0.090	1.630	0.110	1.020	0.070	2.04	0.09	0	2
B012D	0.076	0.033	1.197	0.631	1.899	0.422	2.016	0.485	99.999	99.999	7.27	0.30	2	4
B025D‡	0.250	0.024	4.182	0.955	1.875	1.094	2.463	1.258	0.035	1.008	0.11	0.86	0	3
B026D‡	0.185	0.033	2.467	0.631	1.764	0.422	1.160	0.485	99.999	99.999	0.02	0.30	0	4
B041D	0.126	0.020	0.685	0.851	1.416	0.945	1.897	1.075	1.019	0.817	2.00	0.65	0	3
B043D‡	0.100	0.033	1.661	0.631	1.697	0.422	0.532	0.485	99.999	99.999	0.04	0.30	0	4
B046D‡	0.230	0.026	3.245	1.091	2.712	1.255	3.013	1.454	1.154	1.160	2.15	0.76	0	3
B090D	0.291	0.007	4.122	0.298	2.604	0.349	2.241	0.408	1.732	0.310	1.54	0.23	0	3
B091D	0.112	0.033	2.431	0.631	1.289	0.422	2.117	0.485	99.999	99.999	1.98	0.30	0	4
B111D	0.070	0.033	1.495	0.631	1.014	0.422	1.160	0.485	99.999	99.999	5.73	0.30	2	4
B215D‡	0.187	0.009	2.449	0.392	1.676	0.463	1.450	0.547	1.061	0.414	1.82	0.28	0	3
B240D	0.043	0.033	1.624	0.631	0.179	0.422	0.602	0.485	99.999	99.999	2.01	0.30	7	4
B248D‡	0.286	0.033	3.558	0.631	3.316	0.422	4.468	0.485	99.999	99.999	0.04	0.30	0	4
B257D	0.040	0.033	0.896	0.631	–1.365	0.422	0.036	0.485	99.999	99.999	5.66	0.30	2	4
B289D	0.143	0.033	2.624	0.631	2.565	0.422	–1.270	0.485	99.999	99.999	3.54	0.30	0	4
B292D	0.229	0.033	3.934	0.631	3.381	0.422	0.952	0.485	99.999	99.999	2.15	0.30	0	4
B344D	0.121	0.001	2.517	0.022	2.054	0.024	1.679	0.028	1.372	0.021	2.66	0.02	0	6
DAO25‡	0.060	0.033	2.290	0.631	1.289	0.422	–1.122	0.485	99.999	99.999	1.79	0.30	0	4
DAO30	0.151	0.033	2.273	0.631	3.734	0.422	3.148	0.485	99.999	99.999	3.59	0.30	7	4
DAO47	0.044	0.033	1.179	0.631	–0.033	0.422	3.115	0.485	99.999	99.999	4.20	0.30	2	4
V031	0.052	0.033	1.366	0.631	0.319	0.422	0.812	0.485	99.999	99.999	6.01	0.30	2	4
BA11	0.120	0.033	3.054	0.631	1.697	0.422	0.672	0.485	99.999	99.999	1.07	0.30	0	4
B514	0.062	0.003	0.300	0.137	0.176	0.154	1.279	0.169	0.282	0.159	2.32	0.13	0	7
MCGC1	0.041	0.007	0.566	0.290	0.489	0.327	0.005	0.379	0.397	0.276	1.84	0.29	0	7
MCGC8	0.093	0.003	1.334	0.115	1.400	0.128	1.206	0.147	1.041	0.109	1.98	0.10	0	6
MCGC10	0.031	0.003	0.395	0.104	0.633	0.118	0.427	0.136	0.677	0.100	2.93	0.09	0	6

[1] y = BLCC (young cluster) from Fusi Pecci et al. (2005) 0 – old cluster; 1 – color selected; 2 – H_β selected; 3 – color and H_β selected; 4 – reportedly young objects by other authors and candidates BLCC (Table 2); 7 – classified young by Caldwell et al. (2009).
[2] Dataset label: 0 – Trager et al. (1998); 1 – Puzia et al. (2005); 2 – Beasley et al. (2004); 3 – WHT data; 4 – Perrett et al. (2002); 5 – Huchra et al. (1991); 6 – TNG data; 7 – LOI data.
‡ B025D, B026D, B043D, B046D, B215D, B248D and DAO25 are classified by Caldwell et al. (2009) to be not-clusters and in the following analysis are not considered.

Table A.3. Metallicities for M 31 globular clusters.

Cluster	[Fe/H] dex	e[Fe/H] dex	Cluster	[Fe/H] dex	e[Fe/H] dex	Cluster	[Fe/H] dex	e[Fe/H] dex	Cluster	[Fe/H] dex	e[Fe/H] dex
B001	–0.42	0.32	B085	–2.10	0.26	B183	–0.47	0.15	B344	–0.80	0.21
B003	–0.99	0.48	B086	–1.80	0.18	B184	–0.01	0.22	B347	–1.91	0.24
B004	–1.00	0.41	B088	–1.94	0.52	B185	–0.50	0.20	B348	–0.75	0.23
B005	–0.82	0.38	B090	–0.17	0.26	B187	–1.52	0.54	B350	–1.54	0.31
B006	–0.59	0.41	B092	–1.14	0.23	B188	–1.51	0.51	B352	–0.96	0.24
B008	–0.47	0.35	B093	–0.74	0.38	B190	–0.80	0.39	B356	–1.62	0.32
B009	–1.55	0.23	B094	–0.35	0.30	B193	0.04	0.15	B357	–0.88	0.20
B010	–1.64	0.68	B095	–0.79	0.66	B197	0.02	0.21	B358	–1.85	0.19
B011	–1.71	0.24	B096	–0.23	0.19	B198	–0.55	0.34	B365	–1.32	0.20
B012	–1.91	0.21	B097	–0.95	0.42	B199	–1.70	0.51	B366	–2.14	0.39
B013	–0.74	0.51	B098	–0.45	0.19	B200	–0.43	0.32	B370	–1.98	0.50
B015	0.37	0.15	B099	–0.86	0.36	B201	–1.08	0.16	B372	–1.07	0.53
B016	–0.53	0.34	B103	–0.43	0.15	B203	–0.64	0.36	B373	–0.59	0.47
B017	–0.82	0.24	B105	–0.93	0.42	B204	–0.39	0.15	B375	–0.87	0.22
B018	–0.77	0.39	B106	–0.81	0.28	B205	–1.16	0.15	B377	–1.55	0.33
B019	–0.74	0.15	B107	–1.20	0.15	B206	–1.16	0.15	B378	–1.38	0.51
B020	–0.83	0.15	B110	–0.64	0.28	B207	–1.10	0.44	B379	–0.53	0.15
B021	–0.74	0.37	B111	–0.85	0.71	B208	–0.32	0.30	B381	–1.10	0.22
B022	–1.30	0.59	B112	0.13	0.15	B209	–0.98	0.41	B382	–1.16	0.44
B023	–0.91	0.15	B115	0.06	0.15	B211	–1.92	0.29	B383	–0.47	0.15
B024	–0.59	0.15	B116	–0.50	0.34	B212	–2.07	0.28	B384	–0.59	0.15
B025	–1.53	0.79	B117	–1.78	0.23	B213	–0.69	0.36	B386	–1.09	0.15
B026	–0.09	0.25	B119	–0.25	0.28	B214	–1.00	0.47	B387	–1.37	0.21
B027	–1.64	0.16	B122	–1.20	0.44	B215	–0.33	0.19	B391	–0.96	0.48
B029	0.02	0.21	B125	–1.99	0.34	B217	–0.84	0.39	B393	–1.03	0.24
B030	–0.14	0.26	B126	–1.48	0.19	B218	–0.71	0.18	B397	–0.90	0.22
B031	–1.73	0.39	B127	–0.54	0.15	B219	–0.55	0.26	B398	–0.41	0.18
B032	0.03	0.29	B129	–0.69	0.36	B220	–1.09	0.42	B399	–1.63	0.18
B033	–1.12	0.47	B130	–1.19	0.44	B221	–0.83	0.39	B400	–1.23	0.47
B034	–0.96	0.38	B131	–0.15	0.15	B224	–1.68	0.28	B401	–1.98	0.26
B035	–0.67	0.38	B134	–0.79	0.15	B225	–0.35	0.15	B403	–0.27	0.35
B037	–0.60	0.37	B135	–1.46	0.48	B228	–0.86	0.24	B405	–1.28	0.15
B038	–1.86	0.52	B137	–1.26	0.54	B230	–2.36	0.24	B407	–0.65	0.15
B039	–0.62	0.24	B140	–0.29	0.29	B231	–0.85	0.39	B431*	–1.49	0.33
B041	–1.14	0.47	B141	–1.71	0.58	B232	–2.01	0.23	B457	0.17	0.15
B042	–0.86	0.27	B143	–0.09	0.15	B233	–1.54	0.17	B467	–2.29	0.25
B044	–1.09	0.30	B144	–0.55	0.30	B234	–0.72	0.15	B468	–0.88	0.25
B045	–1.01	0.50	B146	–0.53	0.31	B235	–0.73	0.17	B472	–0.71	0.15
B046	–0.99	0.36	B147	0.02	0.15	B238	–0.43	0.17	B486	–1.91	0.46
B047	–0.28	0.22	B148	–0.70	0.27	B239	–1.46	0.28	B514	–2.06	0.16
B048	–0.55	0.55	B149	–1.00	0.45	B240	–1.74	0.19	G001	–0.73	0.15
B050	–1.21	0.45	B151	–0.44	0.16	B272	–0.81	0.38	G002	–1.63	0.18
B051	–0.73	0.51	B152	–1.53	0.29	B283	–0.52	0.34	G327	–1.79	0.52
B054	–0.10	0.24	B153	–0.13	0.25	B292	–1.54	0.37	NB16	–1.27	0.15
B055	–0.31	0.29	B154	0.03	0.15	B293	–1.59	0.23	NB89	–0.70	0.15
B056	0.07	0.20	B155	–0.08	0.19	B298	–1.78	0.22	B020D	–1.52	0.59
B058	–1.02	0.21	B156	–1.30	0.34	B301	–1.13	0.32	B041D	–1.49	0.74
B059	–0.75	0.40	B158	–0.74	0.15	B304	–1.38	0.33	B090D	–0.09	0.16
B060	–1.13	0.55	B159	–0.77	0.38	B305	–1.04	0.42	B091D	–0.73	0.37
B061	–0.52	0.33	B161	–0.74	0.37	B306	–1.10	0.43	B103D	–0.22	0.27
B063	–0.76	0.17	B162	0.02	0.31	B310	–1.57	0.34	B240D*	–1.74	0.53
B064	–1.37	0.21	B163	–0.08	0.15	B311	–1.71	0.53	B289D	–1.28	0.54
B065	–1.24	0.45	B164	–0.41	0.31	B312	–1.18	0.37	B292D	–0.20	0.27
B068	–0.41	0.17	B165	–1.66	0.29	B313	–0.86	0.19	B344D	–0.64	0.15
B070	–1.42	0.43	B167	–0.25	0.28	B316	–0.79	0.38	DAO30*	–0.26	0.30
B071	0.05	0.24	B169	0.07	0.23	B317	–1.92	0.36	BA11	–0.82	0.40
B072	–0.28	0.29	B171	–0.17	0.15	B328	–2.17	0.30	MCGC1	–2.16	0.28
B073	–0.11	0.25	B174	–1.05	0.22	B335	–0.89	0.40	MCGC8	–1.27	0.15
B075	–1.33	0.46	B178	–1.16	0.21	B337	–1.08	0.15	MCGC10	–2.07	0.15
B076	–0.89	0.40	B179	–0.98	0.27	B338	–1.23	0.22			
B082	–0.55	0.33	B180	–0.75	0.18	B341	–0.96	0.40			
B083	–1.73	0.46	B182	–0.97	0.35	B343	–1.28	0.15			

* Classified young by Caldwell et al. (2009).

Table B.1. Spearman rank correlation coefficients.

	[Fe/H]$_{ZW}$	CN1	CN2	Ca4227	G4300	Ca4455	Fe4531	C24668	Hβ	Fe5015	Mg1	Mg2	Mgb	Fe5270	Fe5335	Fe5709	NaD	TiO1	MgFe
[Fe/H]$_{ZW}$	1.000	0.711	0.620	0.598	0.885	0.684	0.843	0.331	–0.875	0.902	0.912	0.958	0.858	0.860	0.703	0.669	0.772	0.613	0.922
CN1	0.711	1.000	0.961	0.760	0.784	0.537	0.375	0.632	–0.676	0.777	0.703	0.672	0.529	0.527	0.765	0.505	0.627	0.618	0.652
CN2	0.620	0.961	1.000	0.718	0.699	0.566	0.233	0.647	–0.554	0.694	0.618	0.556	0.426	0.424	0.681	0.392	0.537	0.613	0.532
Ca4227	0.598	0.760	0.718	1.000	0.630	0.387	0.301	0.311	–0.542	0.689	0.630	0.600	0.505	0.583	0.632	0.439	0.583	0.637	0.620
G4300	0.885	0.784	0.699	0.630	1.000	0.605	0.664	0.390	–0.868	0.877	0.873	0.855	0.787	0.696	0.659	0.654	0.662	0.576	0.806
Ca4455	0.684	0.537	0.566	0.387	0.605	1.000	0.569	0.238	–0.419	0.755	0.676	0.652	0.667	0.615	0.559	0.279	0.461	0.422	0.630
Fe4531	0.843	0.375	0.233	0.301	0.664	0.569	1.000	0.029	–0.679	0.679	0.706	0.863	0.873	0.814	0.493	0.615	0.598	0.230	0.887
C24668	0.331	0.632	0.647	0.311	0.390	0.238	0.029	1.000	–0.328	0.265	0.365	0.279	0.083	0.056	0.431	0.191	0.191	0.453	0.147
Hβ	–0.875	–0.676	–0.554	–0.542	–0.868	–0.419	–0.679	–0.328	1.000	–0.792	–0.831	–0.873	–0.728	–0.699	–0.659	–0.809	–0.811	–0.495	–0.792
Fe5015	0.902	0.777	0.694	0.689	0.877	0.755	0.679	0.265	–0.792	1.000	0.853	0.887	0.838	0.799	0.775	0.507	0.735	0.657	0.885
Mg1	0.912	0.703	0.618	0.630	0.873	0.676	0.706	0.365	–0.831	0.853	1.000	0.885	0.745	0.721	0.713	0.681	0.752	0.505	0.787
Mg2	0.958	0.672	0.556	0.600	0.855	0.652	0.863	0.279	–0.873	0.887	0.885	1.000	0.922	0.848	0.672	0.647	0.792	0.510	0.946
Mgb	0.858	0.529	0.426	0.505	0.787	0.667	0.873	0.083	–0.728	0.838	0.745	0.922	1.000	0.814	0.596	0.569	0.689	0.444	0.951
Fe5270	0.860	0.527	0.424	0.583	0.696	0.615	0.814	0.056	–0.699	0.799	0.721	0.848	0.814	1.000	0.502	0.502	0.806	0.569	0.892
Fe5335	0.703	0.765	0.681	0.632	0.659	0.559	0.493	0.431	–0.659	0.775	0.713	0.672	0.596	0.502	1.000	0.608	0.593	0.537	0.708
Fe5709	0.669	0.505	0.392	0.439	0.654	0.279	0.615	0.191	–0.809	0.507	0.681	0.647	0.569	0.502	0.608	1.000	0.689	0.208	0.623
NaD	0.772	0.627	0.537	0.583	0.662	0.461	0.598	0.191	–0.811	0.735	0.752	0.792	0.689	0.806	0.593	0.689	1.000	0.480	0.762
TiO1	0.613	0.618	0.613	0.637	0.576	0.422	0.230	0.453	–0.495	0.657	0.505	0.510	0.444	0.569	0.537	0.208	0.480	1.000	0.527
MgFe	0.922	0.652	0.532	0.620	0.806	0.630	0.887	0.147	–0.792	0.885	0.787	0.946	0.951	0.892	0.708	0.623	0.762	0.527	1.000

Appendix B: Spearman correlation matrix for Lick indices and metallicity

During the first phases of the present study we considered the largest set of Lick indices to search for the best candidates to be used as metallicity indicators for our scale. As a useful tool for this choice we computed the matrix of Spearman rank correlation coefficients (Press et al. 1992) for a set of indices in the T98 system and metallicity for Galactic GCs. Since this matrix can be of general interest, we present it here as Table B.1 below. It must be recalled that these correlations coefficients are computed using a sample of nearly-uniformly *old stellar populations*, so it refers only to classical old globulars.